

SIMULATION STUDY OF INTERACTIONS OF SPACE SHUTTLE-GENERATED ELECTRON BEAMS WITH AMBIENT PLASMAS

*Final Report
JN-75-1K
10/74
P. 65*

N93-10066

Unclas

63/75 0121074

FINAL REPORT
NASA Grant NAGW-1936
SwRI Project No. 15-3399

(NASA-CR-190543) SIMULATION STUDY OF INTERACTIONS OF SPACE SHUTTLE-GENERATED ELECTRON BEAMS WITH AMBIENT PLASMAS Final Report (Southwest Research Inst.) 05 0

Prepared by

Chin S. Lin

for
Space Physics Division
NASA Headquarters
Washington, DC 20546

September 30, 1992



SOUTHWEST RESEARCH INSTITUTE
Instrumentation and Space Research Division
6220 Culebra Road, San Antonio, Texas 78238
(512) 684-5111 • FAX (512) 647-4325

**Simulation Study of Interactions of Space Shuttle-Generated
Electron Beams with Ambient Plasmas**

FINAL REPORT
NASA Grant NAGW-1936
SwRI project No. 15-3399

Prepared by

Chin S. Lin

for
Space Physics Division
NASA Headquarters
Washington, D.C. 20546

30 September 1992

Approved by



James L. Burch, Vice President
Instrumentation and Space Research

Table of Contents

I.	INTRODUCTION	1
II.	SUMMARY OF RESEARCH RESULTS	2
III.	LIST OF PUBLICATIONS AND PRESENTATIONS	4
APPENDIX A	Simulations of Radial Expansion of an Injected Electron Beam	
APPENDIX B	Simulations of the Active Injection of Electron Beams	
APPENDIX C	Parameter Study of Electron Beam Injection into an Ionospheric Plasma	
APPENDIX D	Magnetosheath-ionospheric Plasma Interactions in the Cusp: 2. Meso-particle Simulations	

I. INTRODUCTION

This report summarizes results obtained through the support of NASA Grant NAGW-1936. The objective of this project is to conduct large scale simulations of electron beams injected into space. We have completed four papers, including two published in the Proceedings of the 1991 Cambridge Workshop in Geoplasma Physics on Nonlinear Phenomena and Active Experiments. Appendix A presents a published paper entitled "Simulations of radial expansion of an injected electron beam" by J. Koga and C. S. Lin. The other published paper entitled "Simulations of the active injection of electron beams" by Dr. R. M. Winglee is included Appendix B. We also conducted a parameter survey study to examine the dependence of the electron beam radius on various physical variables. The parameter survey results in an article entitled "Parameter study of electron beam injection into an ionospheric plasma" by J. Koga and C. S. Lin. This article is presented in Appendix C.

In addition, applying the injection simulation techniques, we studied the injection of magnetosheath plasma into the cusp. The meso-particle simulations show that magnetosheath plasma injection produces interesting ionospheric plasma outflow from the cusp. We have prepared an article entitled "Magnetosheath-ionospheric plasma interactions in the cusp: 2. Meso-particle simulations" by R. M. Winglee, J. D. Menietti, and C. S. Lin. The article is included in this report as Appendix D. The two articles presented in Appendices C and D will be submitted to Journal of Geophysical Research for publication shortly.

II. SUMMARY OF RESEARCH RESULTS

A. Simulation of Radial Expansion of an Injected Electron Beam

To understand the radial expansion mechanism of an electron beam injected from a highly charged spacecraft, two-dimensional particle-in-cell simulations are conducted for a high density electron beam injected parallel to magnetic fields from an isolated equipotential conductor into a cold background plasma. The simulations indicate that charge buildup at the beam stagnation point causes the beam to expand radially to the beam electron gyroradius.

B Simulations of the Active Injections of Electron Beams

The study of the active injection of electron beams from spacecraft is important as it provides valuable insight into beam-plasma interactions and the development of current systems in the ionosphere. However, the beam injection itself is not simple, being constrained by the ability of the spacecraft to draw return current from the ambient plasma. The generation of these return currents is dependent on several factors including the density of the ambient plasma relative to the beam density, the presence of neutrals around the spacecraft, the configuration of the spacecraft and the motion of the spacecraft through the plasma. Two dimensional (three velocity) particle simulations with collisional processes included are used to show how these different and often coupled processes can be utilized to enhance beam propagation from the spacecraft.

C. Parameter Study of Electron Beam Injection into an Ionospheric Plasma

A parameter study of electron beam injection from a spacecraft into an ionospheric plasma is conducted. The purpose of the study is to survey the simulation parameters for understanding the dependence of beam radius on physical variables. A two-dimensional electrostatic particle code was used to simulate the injection of nonrelativistic electron beams from a finite equipotential conductor into an ionospheric plasma. Due to low background plasma density, the conductor was charged to a higher potential. Beam electrons attracted by the charged conductor were decelerated to zero velocity near the stagnation point which is about two Debye lengths from the conductor. At the stagnation point, the beam electrons receive a large transverse kick and the beam expands radially. The beam electron buildup at the stagnation point produces a large electrostatic force responsible for the transverse kick. The simulations show that the electron beam radius for high spacecraft charging cases is of the order of the beam gyroradius, defined as the beam velocity divided by the gyrofrequency. The parameter survey indicates that the beam radius increases with beam density, and decreases with magnetic field and beam velocity. The beam radius normalized by the beam gyroradius is found to scale according to the ratio of the beam electron Debye length to the ambient electron Debye length. These results are useful for interpreting results of electron beam injection experiments conducted from rockets and the Space shuttle.

D. Magnetosheath-Ionospheric Plasma Interactions in the Cusp

Ionospheric plasma outflow from the cusp can be an important source of plasma to the magnetosphere. One source of free energy that can drive this outflow is the injection of magnetosheath plasma into the cusp. Two-dimensional (three velocity) meso-scale particle simulations are presented which incorporate the interplay between global influences such as the convection of plasma across the cusp, the action of the mirror force and the injection of the magnetosheath plasma combined with wave-particle interactions which produce the actual coupling between the magnetosheath and ionospheric plasmas. It is shown that because the thermal speed of the electrons is higher than the bulk motion of the magnetosheath plasma, an upward current is formed on the equatorward edge of the injection region with return currents on either sides. However, the poleward return currents are the stronger due to convection and mirroring of many of the magnetosheath electrons. The electron distribution in this latter region evolves from upward directed streams to single-sided loss cones or possibly electron conics. The ion distribution also shows a variety of different features depending on its position relative to the injection region due to differences in convection and wave-particle interactions. On the equatorward edge, the distribution has a downflowing magnetosheath component and an upflowing cold ionospheric components due to continuous convection of ionospheric plasma into the region. In the center of the magnetosheath region, heating from the development of an ion-ion streaming instability causes the suppression of the cold ionospheric component and the formation of downward ionospheric streams. Further poleward there is velocity filtering of magnetosheath ions with low pitch angles, so that the ring-beam distribution

are formed and which can produce downward ionospheric conics. These downward components can be eventually turned by the mirror force to produce elevated upwards conic throughout the region after injection.

III. LIST OF PUBLICATIONS AND PRESENTATIONS

1. J. Koga and C. S. Lin, Simulations of radial expansion of an injected electron beam, Proceedings of the 1991 Cambridge Workshop in Geoplasma Physics on Nonlinear Phenomena and Active Experiments, edited by T. Chang, G. B. Crew, and J. R. Jasperse, Scientific Publishers, pp 405, 1992.

2. R. M. Winglee, Simulations of the active injection of electron beams, Proceedings of the 1991 Cambridge Workshop in Geoplasma Physics on Nonlinear Phenomena and Active Experiments, edited by T. Chang, G. B. Crew, and J. R. Jasperse, Scientific Publishers, pp 349, 1992.

3. J. Koga and C. S. Lin, Parameter Study of electron beam injection into an ionospheric plasma, article in preparation.

4. R. M. Winglee, J. D. Menietti, and C. S. Lin, Magnetosheath-ionospheric plasma interactions in the cusp: 2. Meso-scale particle simulations, article in preparation.

5. R. M. Winglee, J. D. Menietti, W. K. Peterson, J. L. Burch, and J. H. Waite, Jr., Magnetosheath-ionospheric plasma interactions in the cusp: 1. Observations of pulsating injections and cold conic suppression, article in preparation.

6. R. M. Winglee, J. D. Menietti, and H. K. Wong, Numerical Simulations of Bursty Radio Emissions From Planetary Magnetospheres, article in preparation.

APPENDIX A

**Simulations of Radial Expansion of
an Injected Electron Beam**

SIMULATIONS OF RADIAL EXPANSION OF AN INJECTED ELECTRON BEAM

J. Koga and C. S. Lin
Aurora Science Inc., San Antonio, TX 78228

ABSTRACT

To understand the radial expansion mechanism of an electron beam injected from a highly charged spacecraft, two-dimensional particle-in-cell simulations are conducted for a high density electron beam injected parallel to magnetic fields from an isolated equipotential conductor into a cold background plasma. The simulations indicate that charge buildup at the beam stagnation point causes the beam to expand radially to the beam electron gyroradius.

I. INTRODUCTION

In this paper we use computer simulations to examine the mechanism by which an electron beam radially expands after injection along magnetic field lines. The subject is of interest because the radial expansion affects the beam diameter and beam density, two critical parameters in determining the beam propagation and the instability conditions of a finite-radius electron beam [1].

Several two-dimensional simulations show that high density electron beams can propagate in a plasma because the net beam charge has caused the beam to expand radially and reduced the beam density [2–5]. For cross-field injection the beam is found to form a hollow cylinder of radius approximately equal to the beam electron gyroradius ρ_b , defined as the beam velocity v_b divided by the electron gyrofrequency Ω_{ce} [3]. In the case of parallel injection, the beam expands to fill a cylinder with a radius smaller than ρ_b . However the radial expansion mechanism remains unclear for parallel beam injections. This paper reports our simulation results about the radial expansion mechanism of an electron beam injected parallel to magnetic fields. In contrast to [4], we concentrate on the cases of high spacecraft charging.

† Present address: Aurora Science Inc., San Antonio, TX 78228.

II. SIMULATION RESULTS

Realistic modeling of beam injection from a spacecraft requires injecting an electron beam from a finite isolated conductor. Using the capacity matrix method [4,6], we treat the spacecraft surface as a finite isolated equipotential conductor in an ambient plasma.

The simulation system contains 512×128 cells in the x and y coordinates. We use a periodic boundary condition for the lower and upper boundaries, and assume that the electric field at the left boundary and the potential at the right boundary are zero. The spacecraft is represented by a rectangular box centered at $x = 102\Delta$ and $y = 64\Delta$ with a size of $4\Delta \times 32\Delta$ in the x and y directions, respectively. The grid size, Δ , equals the Debye length of the ambient electrons defined as $\lambda_d = a_c/\omega_{pe}$ where $a_c = (2T_e/m_e)^{1/2}$ is the thermal velocity of the ambient electrons. ω_{pe} is the ambient electron plasma frequency, and T_e is the ambient electron temperature. The ratio of ion to electron mass is 100, and $a_c = 0.001c$ where c is the speed of light, a unit of the simulation. The electron gyrofrequency Ω_{ce} is chosen to be $0.25\omega_{pe}$, close to the ionospheric value of $0.3\omega_{pe}$. The simulations have a time step $\Delta t = 0.05\omega_{pe}^{-1}$ and 131,072 particles for the ambient plasma. We have chosen the simulation parameters such that the beam has a density n_b much greater than the background density n_c ($n_b \gg n_c$) and a beam velocity much larger than the background thermal velocity ($v_b \gg a_c$). In the simulations, the electron beam has a width of 4Δ , an injection velocity of $v_b = 10a_c$ along the x axis, zero initial thermal velocity, and a density ratio of $n_b/n_c = 10$.

Figs. 1–3 show the simulation results at $\omega_{pe}t = 30$ when the simulations end. Fig. 1a plots beam electrons in the $v_x - x$ phase space, indicating that a large number of beam electrons are held close to the conductor surface. From a more detailed examination of the particle velocities near the conductor surface, we deduce that the stagnation point, where the injected electron velocity is significantly reduced, lies at about 2Δ away from the conductor surface.

Due to the high beam density the spacecraft becomes positively charged, causing the beam electrons to be rapidly drawn back to the spacecraft surface. The average electrostatic potential of the spacecraft in this case is $\approx 95\%$ of the beam energy. Some electrons at the front of the beam are accelerated to velocities higher than the original beam velocity, due to the bunching of beam electrons behind the beam head. Also some beam electrons returning to the conductor overshoot the conductor to the wake side. The configuration space plot (Fig. 1b) shows that the electron beam

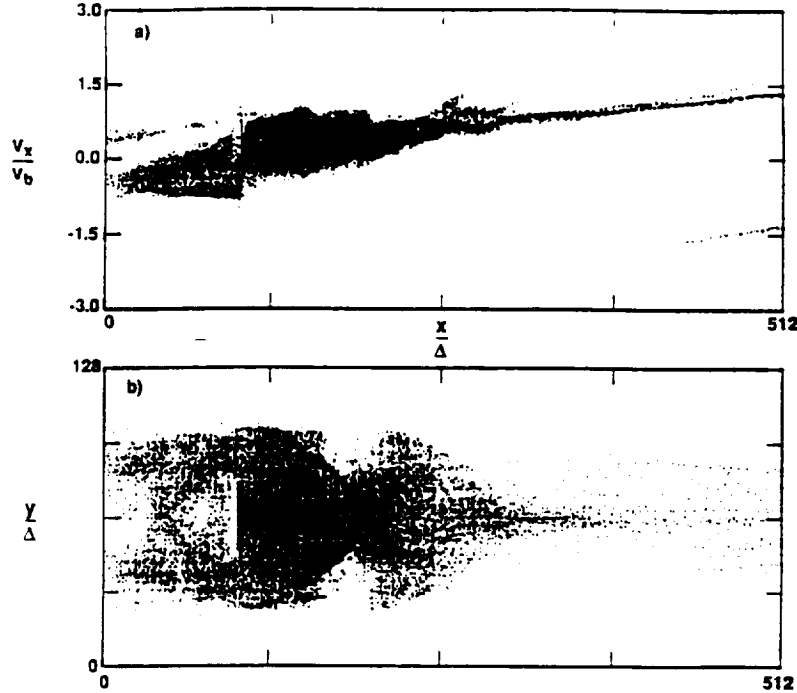


Figure 1. Simulation results for $n_b/n_c = 10$ and $v_b/a_c = 10$ at $\omega_{pe}t = 30$: (a) the phase space plot of the beam electrons in the $v_x - x$ coordinates and (b) the configuration plot of the beam electrons showing the electron positions in the $x - y$ plane.

expands radially. It appears that the maximum beam expansion occurs immediately after the stagnation point.

A contour plot of the beam density is presented in Fig. 2, where the outer contour line specifies the boundary of zero beam density and the inner contour line specifies 10 beam electrons per cell (shaded area). The shaded area for high beam density is a small region very close to the conductor, which is represented in the figure as a vertical slit. Based on the contour plot, we deduce that the beam radius r_b is about 40Δ , approximately equal to the beam electron gyroradius ρ_b .

The bottom panel of Fig. 2, which plots the beam density averaged over the y coordinate versus x , further illustrates the concentration of beam electrons around the conductor surface. The beam density is highest at the stagnation point, in agreement with analytical results for one-dimensional electron beam injection into a vacuum [7]. Physically, the beam density profile can be qualitatively explained by the conservation of flux $n_b v_b$. Because the average beam velocity is smallest at the stagnation point, the beam density should reach its maximum value there. However, beyond the

stagnation point, the beam density decreases as the beam expands transversely and the average beam velocity increases.

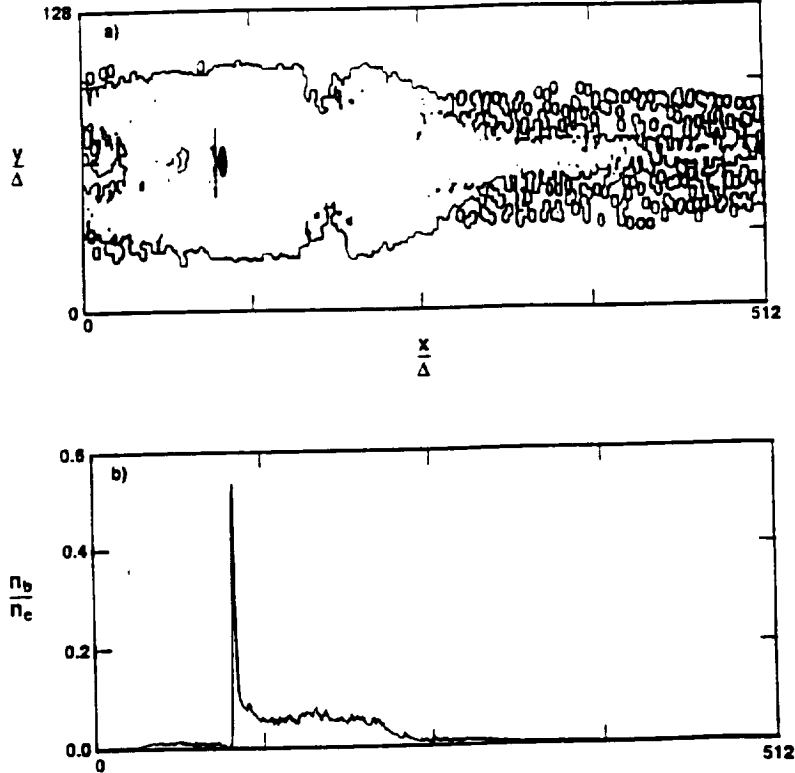


Figure 2. (a) Density contours of the beam electrons at $\omega_{pe}t = 30$. The outer contour line delineates the beam envelope and the small shaded area has more than 10 beam electrons per cell. The vertical slit near the shaded contour line represents the conductor. (b) profile of the beam density averaged over y .

To further understand the mechanism of radial expansion, we examine the transverse electric field E_y and the longitudinal electric field E_x . At each x coordinate, we find the maximum values of E_y and E_x along the y coordinate and plot them as a function of x (Figs. 3a and 3b). Comparing Figs. 3a and 3b with Fig. 2b, we note that the maximum transverse electric field E_y and the maximum longitudinal electric field E_x occur at the stagnation point, where the beam density is highest. The electric field profiles thus imply that the beam electrons gain their transverse velocities mainly in the stagnation region. In general beam electrons travel through the stagnation region with velocities much lower than the initial beam velocity. So they spend more time in the stagnation region and are accelerated to higher velocities. After the stagnation region the transverse electric field E_y is smaller (Fig. 3a) and the average beam velocity is higher (Fig. 1a).

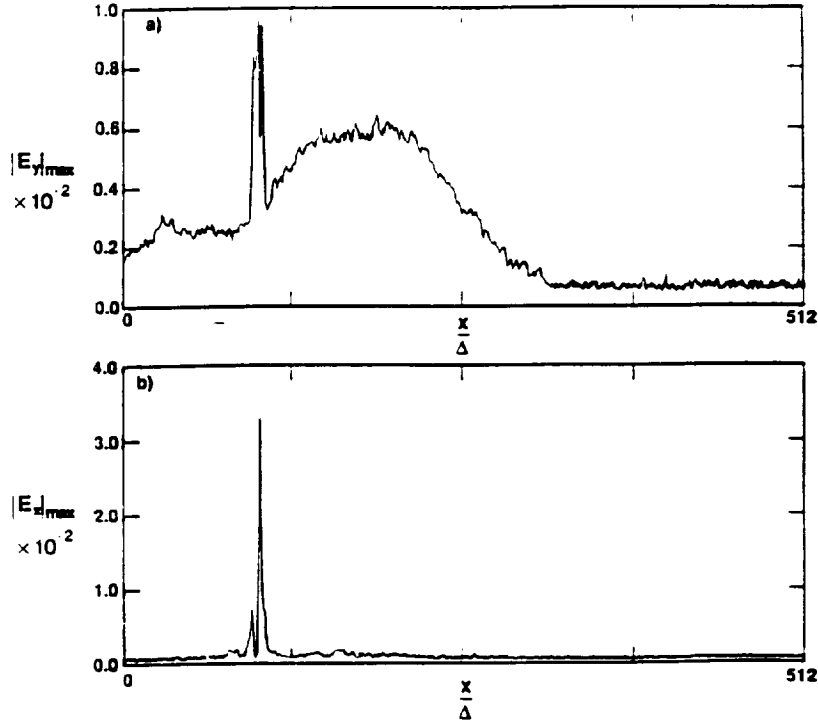


Figure 3. Profiles of the maximum transverse electric field (top) and the maximum longitudinal electric field (bottom). The maximum values are determined from a column of cells at each given x position.

Therefore, the beam electrons receive their largest transverse kick very close to the spacecraft and experience smaller transverse acceleration from that point on.

The transverse velocities to which the beam electrons are accelerated depend on E_y and the duration the beam electrons spend in the stagnation region. The width of the large transverse electric field region is approximately 8Δ (Fig. 3a). From the maximum value of E_y and the average beam velocity in the large electric field region, we estimate that the beam electrons can gain a transverse velocity about $0.75v_b$. In the simulations the beam electron velocity v_y immediately after the stagnation point has a maximum value about v_b . As a result, the radius of the beam envelop is of the order of the beam electron gyroradius.

III. SUMMARY

We have examined the radial expansion mechanism of a high density electron beam injected parallel to magnetic fields into a background plasma. The simulations indicate that in high beam current cases ($n_b \gg n_c$)

and $v_b \gg a_c$), the beam radius expands to the beam electron gyroradius. Previous simulations have indicated that the radius of a parallelly injected electron beam expands to about half the beam electron gyroradius for $n_b = 4n_c$ [4]. We have conducted a parameter survey to determine the dependence of the beam radius on beam density and other plasma parameters. Due to page limitation, the results will be reported separately.

The radial expansion is found to occur near the stagnation point, very close to the conductor surface for our parameters. It appears that the initial expansion determines the beam envelope after the stagnation point. The radial expansion is shown to be caused by charge buildup at the stagnation point, producing locally a large transverse electric field. Accelerated by the transverse electric field, the beam electrons injected parallel to magnetic fields receive a large transverse kick. The maximum perpendicular velocity gained by the beam electrons approaches the beam injection velocity.

In this paper we have concentrated on high beam current simulations relevant to significant spacecraft charging. Note that the conductor potential in our simulations reaches about 95% of the beam energy. The simulation results are thus most applicable to the SEPAC electron beam injection experiments on the Shuttle when it was charged to the beam energy.

ACKNOWLEDGEMENTS

We would like to thank R. M. Winglee for helpful suggestions on simulation techniques. The work was supported by NASA contract NAGW-1936 and by Lewis Research Center through NASA Contract NAS8-32488. The particle simulations were performed on the CRAY-YMP at NASA Ames Research Center and the CRAY-YMP at Goddard Space Flight center.

REFERENCES

- [1] H. K. Wong and C. S. Lin, *Radio Sci.*, **25**, 277, (1990).
- [2] R. M. Winglee and P. L. Pritchett, *J. Geophys. Res.*, **92**, 6114 (1987).
- [3] H. Okuda and J. Berchem, *J. Geophys. Res.*, **93**, 175 (1988).
- [4] R. M. Winglee, and P. L. Pritchett, *J. Geophys. Res.*, **93**, 5823 (1988).
- [5] C. S. Lin and J. K. Koga, *IEEE Trans. Plasma Sci.*, **17**, 205 (1989).
- [6] R. W. Hockney and J. W. Eastwood, *Computer Simulation Using Particles* (McGraw-Hill, New York, 1981).
- [7] D. E. Parks, A. R. Wilson, and I. Katz, *IEEE trans. Nucl. Sci.*, **NS-22**, 2368 (1975).

APPENDIX B

Simulations of the Active Injection of Electron Beams

SIMULATIONS OF THE ACTIVE INJECTION OF ELECTRON BEAMS

R. M. WINGLEE

Department of Space Sciences, Southwest Research Institute
PO. Drawer 28510, San Antonio, TX 78228-0510

ABSTRACT

The study of the active injection of electron beams from spacecraft is important as it provides valuable insight into beam-plasma interactions and the development of current systems in the ionosphere. However, the beam injection itself is not simple, being constrained by the ability of the spacecraft to draw return current from the ambient plasma. The generation of these return currents is dependent on several factors including the density of the ambient plasma relative to the beam density, the presence of neutrals around the spacecraft, the configuration of the spacecraft and the motion of the spacecraft through the plasma. Two dimensional (three velocity) particle simulations with collisional processes included are used to show how these different and often coupled processes can be utilized to enhance beam propagation from the spacecraft.

I. INTRODUCTION

Over the past ten years there have been several space experiments which utilize electron beams injected from spacecraft to study beam-plasma interactions and the development of current systems in space plasmas. Recent or continuing active experiments which employ electron beams include: (i) the ECHO program [1-6], (ii) the Space Experiments with Particle Accelerators, SEPAC, and the Vehicle Charging And Potential, VCAP, experiments on the Space Shuttle [7-13], (iii) MAIMIK [14-15] and (iv) the Cooperative High Altitude Rocket Gun Experiments, CHARGE [16-18].

While understanding the characteristics of the beam-plasma interaction and the induced currents is central to the above experiments, there are fundamentally important differences in the beam and spacecraft configuration which can significantly alter the characteristics of the interaction between the different experiments. For example, in the early experiments the beam was injected from a single spacecraft where most of the diagnostics were confined. As it became more evident that significant spacecraft charging could be occurring and that effects from the beam-plasma interaction were not restricted to just the beam region, the emphasis in the more recent experiments has been to investigate the induced plasma phenomena via diagnostic packages ejected from the beam-emitting (mother) payload.

If in addition, these ejected payloads remained electrically connected via a tether wire, spacecraft charging could conceivably be reduced by the collection of current by the ejected payload at extended distances across the field lines. Such a tethered (daughter) payload was successfully deployed during CHARGE 2. Tethered payloads were also successfully deployed during Echo 7 and MAIMIK but in these experiments the tether impedance was made very high in order to measure the potential across the field lines rather than to collect current.

The results of CHARGE 2 are particularly interesting because they showed that in the absence of neutrals the percentage of current collected by the daughter payload tended to be smaller than its relative area, i.e. that the tethered payload is relatively inefficient in collecting current [18]. However, during thruster firings from the daughter payload, the daughter could collect a large fraction of the beam current. This current collection could be suppressed during thruster firings from the mother payload, irrespective of whether neutrals were being injected from the daughter.

Understanding the above results is not only important in itself but could possibly have important applications for the upcoming Shuttle Electrodynamics Tether Satellite (SETS). In this experiment, a satellite will be released from the shuttle along a tether that can extend up to 10 km. Power can be generated via the motion of the tether wire through the geomagnetic field if the tether current can be closed in the ionosphere via beam injection. While the geometry of SETS is very similar to that of CHARGE 2, one important difference is that in the sounding rocket experiments, the payloads are subsonic, moving at about 1 km/s, while the shuttle travelling at about 8 km/s is supersonic. As a result of this supersonic propagation, the current collecting characteristics of the spacecraft can be modified.

The purpose of this paper is to investigate the processes governing the return currents into the spacecraft for the different configurations to identify that configuration which best enables the beam to propagate away from the spacecraft with minimal distortion. The study utilizes two-dimensional (three velocity) electromagnetic particle simulations to self-consistently evaluate the current and beam characteristics as well as the heating of the ambient plasma as functions of (a) the spacecraft configuration, (b) the injection of neutrals and (c) the motion of the spacecraft through the ambient plasma.

II. SIMULATION MODEL

The algorithm for the particle simulations is described in [20, 21]. These simulations allow the self-consistent evaluation of the beam-plasma interaction as well as effects from spacecraft charging and the ionization of neutrals. Schematics for the different spacecraft configurations considered are shown in Figure 1. The mother and daughter payloads are indicated by

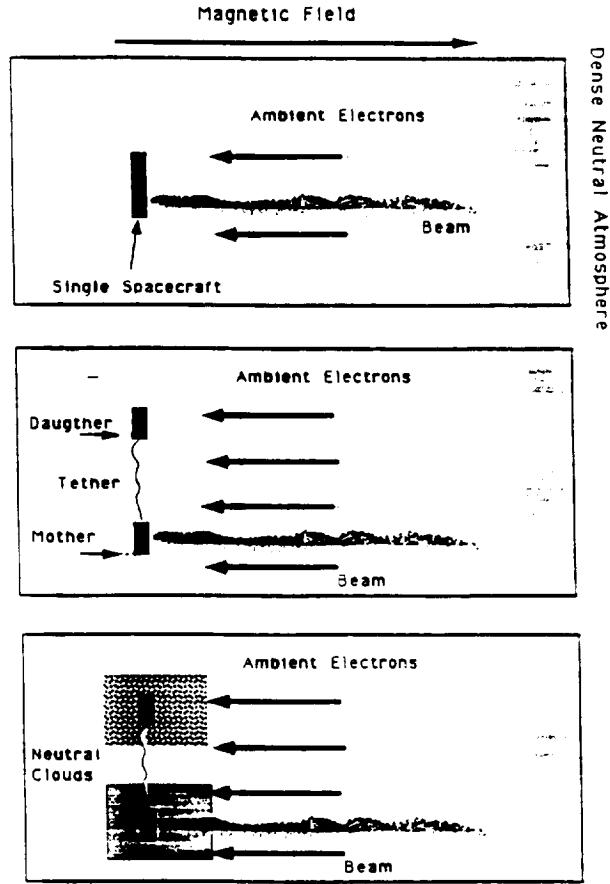


Fig. 1. Schematic showing the different spacecraft configurations. considered

the black rectangles and are of equal size with dimensions $4\Delta \times 16\Delta$ where the system size is $512\Delta \times 128\Delta$ and Δ is a plasma Debye length which is of the order of 10 cm for the parameters considered here. For the single spacecraft configuration, the two payloads are placed side-by-side (Fig. 1a) with both payloads kept at the same potential. The beam is injected from the middle of the lower (mother) payload at an angle of 45° to the magnetic field which is in the x-direction. The parallel velocity of the beam is assumed to be 10 times the ambient thermal velocity (i.e., $v_{zb} = 10v_{Te}$). Because of the limited resolution of the simulations the beam density is assumed to be smeared out over a slightly larger region than the actual beams used in the experiments and the beam density is correspondingly reduced so that the total beam current is comparable to that used in the CHARGE 2 experiment, i.e., about 100 mA. In the following, the beam width is taken to be 2Δ and the beam density density is assumed to be 4 times the ambient density which is of the order of 10^5 cm^{-3} , similar to [22]. The corresponding ambient plasma frequency ω_{pe} is equal to the

electron cyclotron frequency Ω_e and the (initial) beam plasma frequency ω_{pb} is equal to $2\omega_{pe}$.

For the tethered configurations, the mother and daughter payloads are separated by 64Δ across the field lines. With this separation, return currents can be generated over a larger distance across the field lines (Fig. 1b). Charge is moved between the two payloads so that both spacecraft are maintained at the same potential, essentially modelling the role of the tether wire. In addition, a voltage can be applied between the two payloads to shift in the potential of the payloads relative to the plasma potential and thereby modify their current collection capabilities.

As discussed in the following sections, the local plasma can become depleted due to return currents into the spacecraft, leading to the strong charging of the spacecraft, irrespective of the above spacecraft configurations. However, this plasma depletion can be overcome by the injection of neutrals and their ionization by energetic electrons (Fig. 1c). For simplicity, the neutral cloud is assumed to extend 50Δ behind the spacecraft and 100Δ in front with a width of 32Δ and a density of about 10^{11} cm^{-3} . This neutral cloud can be placed around either the mother or daughter.

III. BEAM INJECTION IN THE ABSENCE OF NEUTRALS

The evolution of the beam phase space for the single spacecraft and tether configurations are shown in Fig. 2. For the single spacecraft configuration, a stagnation region where some of the beam electrons are decelerated and eventually drawn back into the spacecraft (i.e., beam electrons with $v_z < 0$) quickly forms but, with neutralization by the return currents from the ambient plasma, some of the beam particles are able to escape and there is strong heating of the beam particles due to induced turbulence (Fig. 2a). At later times, the ambient plasma becomes depleted leading the reformation of the stagnation region (Fig. 2b). This stagnation region then remains a permanent feature until the beam is turned off (Fig. 2c) [20].

For the tether configuration, the beam is more easily able to propagate away from the spacecraft at early times (e.g., Figs. 2d and e). This enhanced propagation is due to the increased area over which return currents are drawn from the plasma when the payloads are separated across the field lines. Nevertheless, the local ambient plasma eventually becomes depleted as before and a stagnation region eventually forms (Fig. 2f). This depletion also occurs even if the daughter is biased positively and the mother negatively (phase spaces not shown). Thus, while the tether configuration allows enhanced current collection initially, the local depletion of plasma still leads to strong spacecraft charging and beam distortion.

The ability of the different payloads to collect current is illustrated in Fig. 3 which shows the time history of the relative current collected by

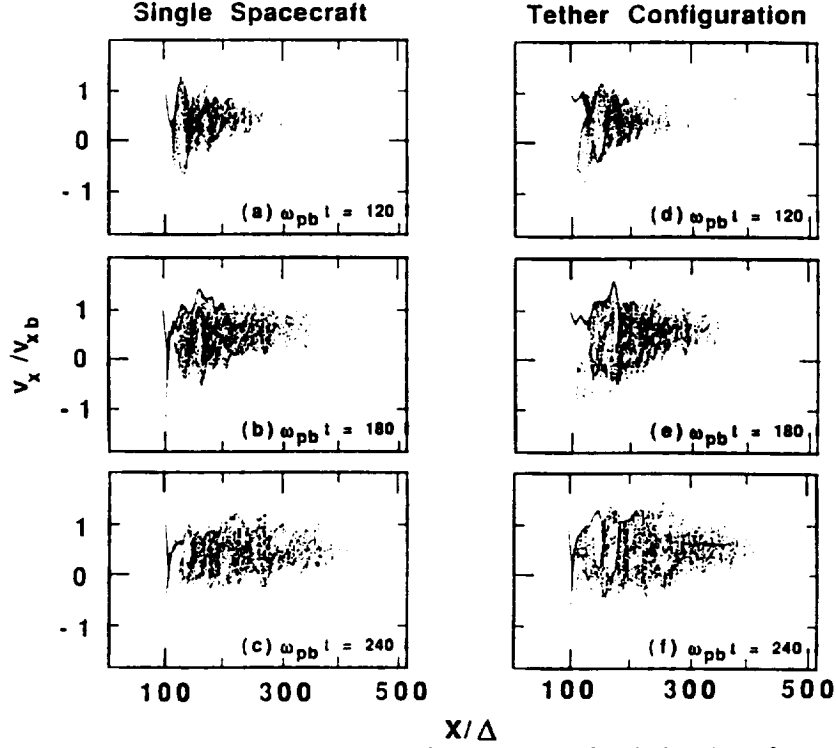


Fig. 2. The evolution of the beam phase space for injection from a single spacecraft (left hand side) and from a tethered configuration (right hand side).

the two payloads. In all cases, the beam is turned off at $\omega_{pb}t = 240$. For the single spacecraft configuration (Fig. 3a), it is seen that the daughter initially collects about 30% of the beam current even though it has the same surface area as the mother. The relative fraction collected by the daughter increases to a maximum of about 50% of the beam current at $\omega_{pb}t \simeq 120$, after which the depletion of the ambient plasma leads to a drop off in current collected. At this point the current collected by the mother increases. Much of this return current is, however, made up of reflected beam particles (as seen from the phase spaces in Fig. 2). After beam turn-off there is a rapid drop out in this component. However, the spacecraft continues net negative charge for about $60/\omega_{pb}$ after turnoff which causes the spacecraft to reach high negative potentials after beam turnoff.

For the tethered configuration (Fig. 3b), the amount of return current collected by the daughter increases until about $180/\omega_{pb}$, which is about a 50% increase on the period seen in the single spacecraft configuration. The current collected by the daughter can be further enhanced by making the daughter positively biased and the mother negatively biased. This enhancement is illustrated in Fig. 3c. In this case, the daughter is able to collect nearly 0.8 of the beam current during the first half of the beam

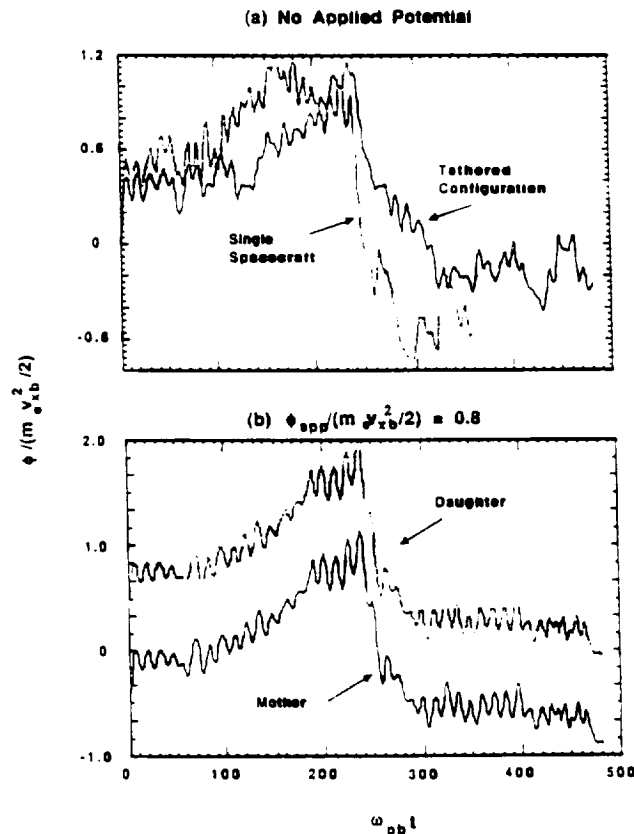


Fig. 3. Time histories of the current collected by the daughter (dotted lines) and the mother (solid lines) for (a) the single spacecraft configuration, (b) the tether configuration and (c) when a voltage equal to 80% of the parallel beam energy is applied between mother and daughter. The beam is turned off at $\omega_{pb} t = 240$.

injection. However, in both cases the depletion of the local plasma leads to a drop out in the daughters ability to collect current.

Fig. 4 shows the time histories of the potentials of the mother and daughter corresponding to Fig. 3. In all cases, when the local plasma becomes depleted, the potential of the beam-emitting payload increases to about the parallel energy of the beam. This is true even if a potential is applied between the payloads to make the initial potential of the beam-emitting payload negative.

IV. BEAM INJECTION IN THE PRESENCE OF NEUTRALS

The above results show that the depletion of the ambient plasma can lead to strong spacecraft charging. This effect can be offset with the injection of neutral (e.g., during thruster firings) and the subsequent ionization by energetic electrons can lead to the replenishment of the ambient plasma. This effect is well documented experimentally [18] and has been

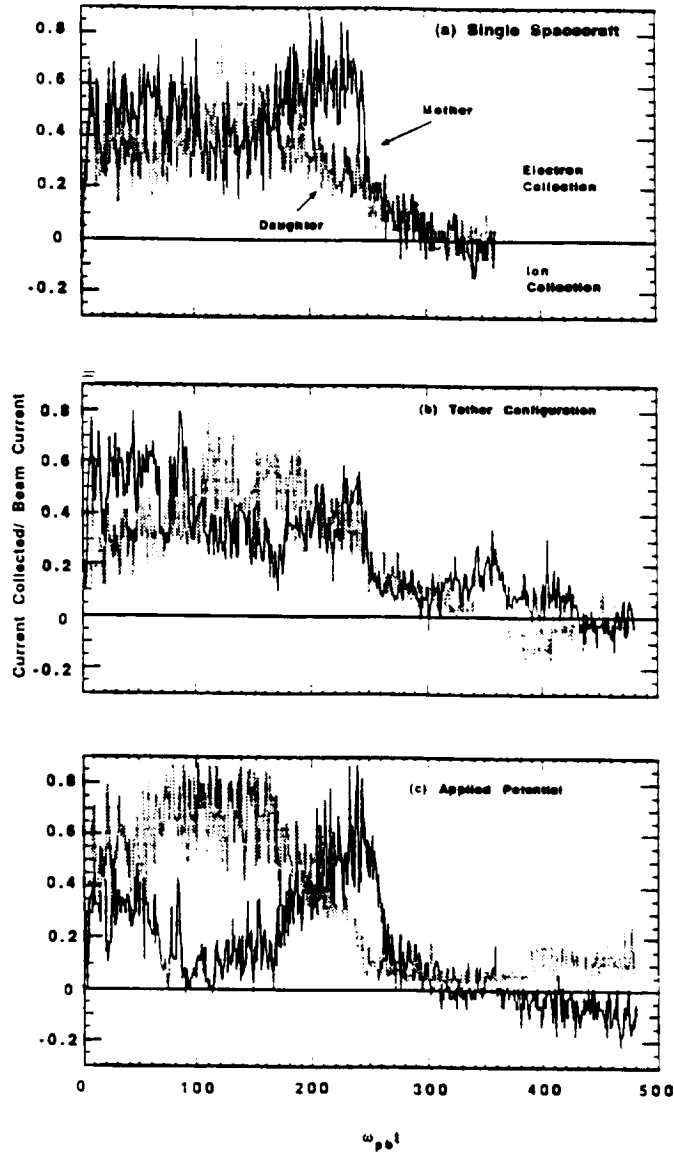


Fig. 4. Time histories of the spacecraft potential for the cases shown in Fig. 3.

recently investigated via particle simulations for the single spacecraft configuration [21]. In this section, the simulations are extended to the tether configuration. The same voltage as in Fig. 4b is applied between mother and daughter.

For these ionization processes to be important, the collision period must be comparable to or smaller than the time for the stagnation region to form. For the present parameters, the stagnation region forms in $\omega_{pb}t \lesssim 200$ so that for ionization processes to be important the collisional frequency ν_c must be greater than about $0.005\omega_{pb}$. In the following, ν_c is set at $0.01\omega_{pb}$. The corresponding evolution of the beam phase is shown in Fig. 5 when the

neutral are injected around the mother (left hand side) and the daughter (right hand side).

It is seen that in both cases a well defined stagnation region does not form. Instead, when the neutrals are around the mother payload, there is direct ionization by beam particles which rapidly builds a high density plasma of moderate energy in the beam region (as seen by the high phase space density in the region $100 \lesssim x/\Delta \lesssim 200$ and $-0.5 \lesssim v_x/v_{xb} \lesssim 0.5$). This latter plasma can be drawn into the spacecraft to provide return current if the mother payload becomes positively charged to overcome the slight net forward momentum of the ionized electrons.

While placing neutrals in the beam region is efficient in reducing the level of spacecraft charging, it has the disadvantage that it also leads to the development of strong turbulence in the beam region that cause the beam to loose its coherence. This turbulence is seen in Fig. 5a-c as the development of short scale length vortices. It has relatively short scaled length because the newly ionized plasma increases the local plasma frequency so that resonant interactions between beam and plasma particles is forced to move to higher k values.

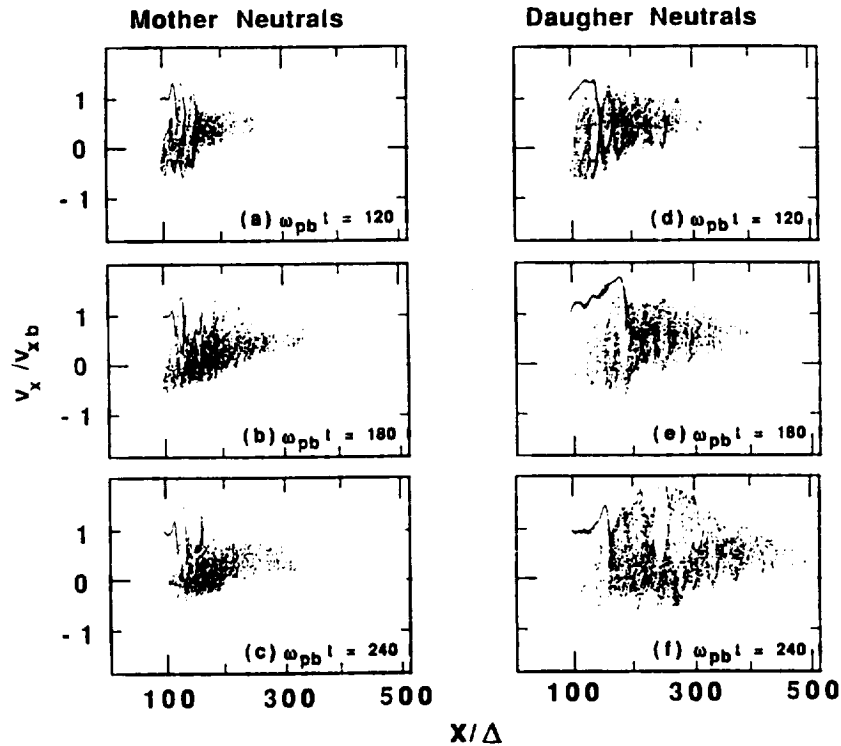


Fig. 5. The evolution of the beam phase space for the tether configuration with neutrals injected around the mother (left hand side) and from the daughter (right hand side).

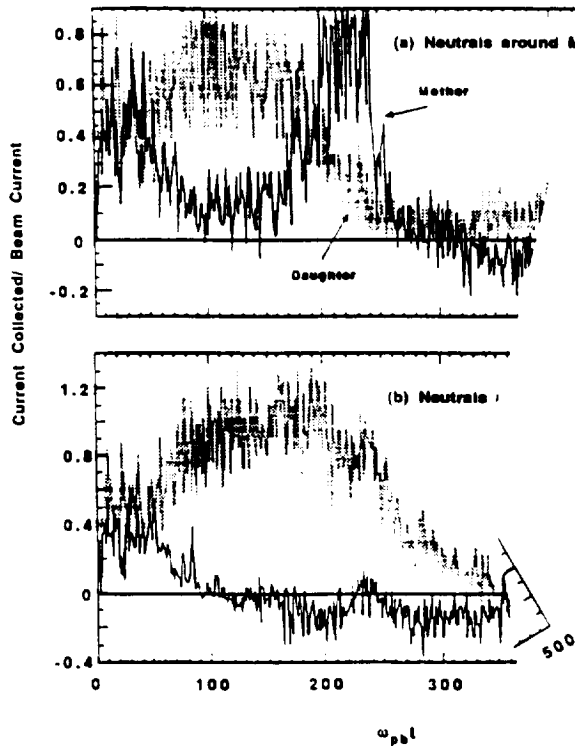


Fig. 6. The time histories of the payload potentials corresponding to the beam phase spaces in Fig. 5.

If instead, the neutrals are placed around the daughter payload then ionization can occur via vehicle induced ionization, i.e. if the daughter has a sufficiently high positive potential that the return current electrons attain ionization energies. This can be achieved by applying a voltage across the tether to make the daughter positively charged (in the present case to a few hundred volts). This method has the advantage that not only is the spacecraft charging reduced but it also minimizes beam distortion since the newly created plasma is well away from the beam region. This is seen in Figs. 5d and e where much of the beam is seen to propagate well away from the spacecraft with much less turbulence than seen in the counter parts for the mother-neutral case; at beam turn-off (Fig. 5f) a well defined beam is still seen out to $x/\Delta \simeq 300$ despite some induced turbulence.

The corresponding evolution of the spacecraft potential is shown in Fig. 6. As noted above, the case where the neutrals are injected around the mother, the mother has to charge to a sufficiently positive potential to draw the newly created plasma into the spacecraft. In the present case because the ionization threshold is set at three times the ambient thermal speed, the required potential is about a third of the beam energy, which is consistent with the simulation results. When more realistic ionization thresholds are utilized, the potential attained by the mother payload should be much

smaller. For the case when the neutrals are injected from the daughter, the return current can actually exceed the beam current (particularly when there is a high positive potential applied to the daughter), resulting in a decrease in the potential of both mother and daughter. As a result, the mother can be maintained at a low, even negative, potential during beam injection.

V. EFFECTS FROM THE MOTION OF THE SPACECRAFT

In the above simulations, the payloads were assumed stationary during the beam injection. This is not a restrictive assumption for sounding rocket experiments. However, because of the much higher speed of the space shuttle, ram and wake effects can develop which can possibly modify the beam-plasma interaction as well as the charging of the spacecraft. These effects are now examined through a comparison between the results from a stationary tether configuration (with no applied voltage) and when the mother and daughter payloads are moving across the field lines at a speed equal to twice the sound speed. In both cases, the mother and daughter are assumed to be initially separated by 32Δ .

One advantage of the motion of the spacecraft is that additional plasma can be swept into the spacecraft and help reduce the level of spacecraft charging. However, this is a relatively weak effect even when the spacecraft are travelling at twice the sound speed as illustrated in Fig. 7a. At early times when effects from the local depletion of the ambient plasma are small, the spacecraft potentials are approximately equal. However, after about $\omega_{pb}t \simeq 100$, the potential for the stationary spacecraft starts to increase at a faster rate than the potential for the moving spacecraft, reaching the beam energy at about $\omega_{pb}t \simeq 200$. The potential for the moving spacecraft remains below the beam energy throughout the period of injection and is about 20% below that of the stationary spacecraft at turnoff.

With the reduction in the spacecraft charging, the beam is able to generate slightly enhanced electromagnetic radiation as seen in Fig. 7b. Again this is only about a 20% increase for spacecraft moving at mach 2. The beam is also better able to propagate into the plasma, although it is again only a small change. This difference in beam propagation is illustrated in Fig. 8 which shows a full perspective of the beam phase space at $\omega_{pb}t = 180$ for injection from stationary spacecraft (left hand side) and from supersonic spacecraft. The bottom panels show the density of particles in the x - y plane, while the left and right panels show the v_x - x and v_x - y phases spaces, respectively. For the case of stationary spacecraft, there is strong reflection of beam particles at $x/\Delta \simeq 200$ (as indicated by the dashed line in the v_x - x panel) whereas this reflection occurs at about $x/\Delta \simeq 250$ for the case of supersonic spacecraft. In addition by $\omega_{pb}t = 240$

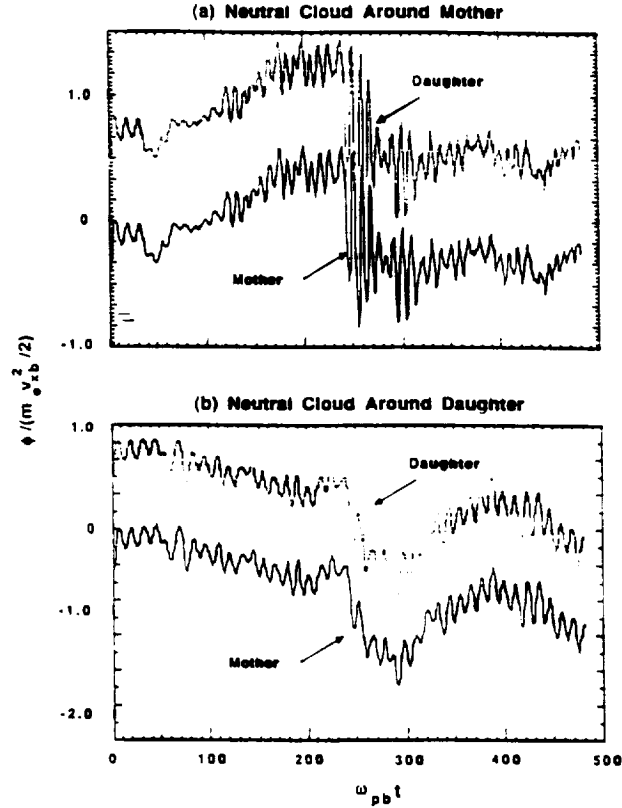


Fig. 7. Time histories of (a) the spacecraft potential and (b) the induced magnetic field for stationary spacecraft (dotted lines) and when the spacecraft are moving across the fields lines at twice the sound speed (solid lines).

(not shown), a well defined stagnation regions forms in the earlier case while in the latter case it is only just beginning to form.

Despite this enhanced penetration, beam distortion is enhanced via the increased turbulence induced by the motion of the spacecraft. For example, in both cases a sinusoidal trace is seen in the x - y panel near the spacecraft as the beam gyrates about the magnetic field. For the case of the stationary spacecraft, about one and a half gyrations can be identified in the density phase space before being smeared by turbulence while only about three quarters of a gyration can be seen on the right hand side. This enhanced turbulence is also seen in the v_x - x panels where there is stronger filling in of the phase space (particularly in the region $100 \lesssim x/\Delta \lesssim 200$) for the moving spacecraft. This difference arises because, for stationary spacecraft, the newly injected beam particles interact with essentially the same plasma so that at late times there is some saturation of the beam-plasma interaction. For injection from supersonic spacecraft, the newly injected

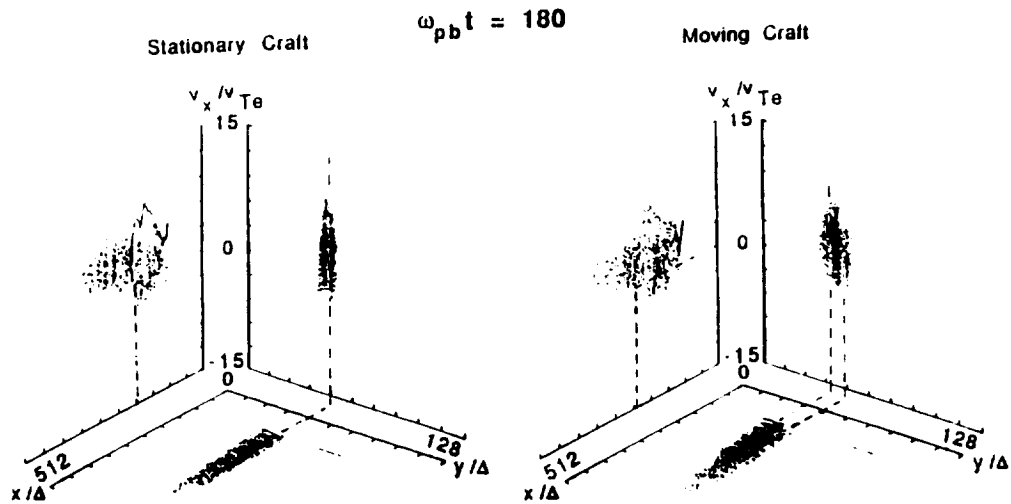


Fig. 8. Plots of the beam parallel velocity phases for injection from stationary spacecraft (left hand side) and from moving spacecraft (right hand side). The plot panels show density in coordinate space while the right and left hand panels show the v_x - x and v_x - y phase spaces, respectively.

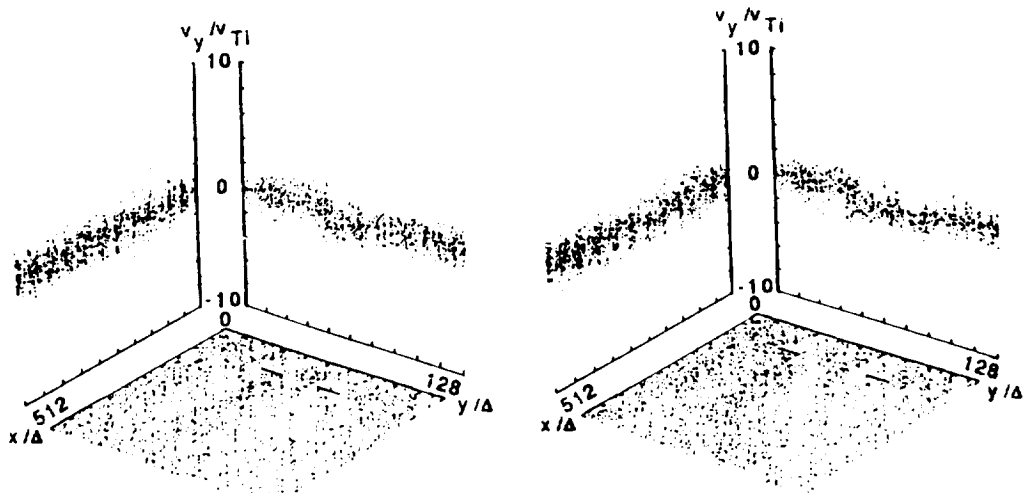


Fig. 9. As in Fig. 8, except for the ambient ion perpendicular velocity v_y .

beam particles interact with slightly different plasma, thereby allowing continual growth of the turbulence, albeit in slightly different regions.

Due to the presence of the enhanced turbulence, the highest energy beam particles are seen in the ram side of the beam as seen from the v_x - y panels. In the wake side, the energy of the beam particles is rapidly dissipated and the average speed of the particles is about 50% of that in the ram. Some of the beam particles which have been back-scattered and are in the wake miss the spacecraft before it moves across the field lines so that some of the beam particles propagate behind the spacecraft.

Probably the strongest effect associated with the motion of the spacecraft is in the heating and acceleration of the ambient ions, as illustrated in Fig. 9 which shows the ion perpendicular velocity v_y in the same format as Fig. 8. In both cases, as the beam is injected, the plasma ions are swept into the beam region to provide charge neutralization of the beam particles which have higher density than the ambient plasma [cf. *Winglee and Pritchett, 1988*]. This is seen as an enhancement in the ion density in the beam region in the x - y panels and, in the v_y - y panels as a positive acceleration in v_y for ions below the beam region (i.e. $y/\Delta \lesssim 32$) and a negative acceleration for ions above the beam region. These latter ions in the case of supersonic spacecraft are moving in the same direction as the spacecraft. As a result, those ions which have velocities comparable to the spacecraft experience an additional pull or acceleration as the beam regions moves across the field lines with the spacecraft. In the present example, these latter ions attain a maximum speed nearly twice that seen when the spacecraft are stationary.

VI. SUMMARY

In this paper, two-dimensional (three velocity) particle simulations have been used to investigate the injection and propagation of electron beams from spacecraft for a variety of different experimental configurations relevant to several recent and ongoing active beam experiments. These different configurations include injection from (i) a single spacecraft, (ii) a pair of electrically connected or tethered spacecraft, (iii) spacecraft immersed in high density neutral clouds and (iv) moving spacecraft.

It has been shown that in the absence of high density neutrals around the spacecraft, the local depletion of the ambient plasma via return currents into the spacecraft leads to the eventual strong charging of the spacecraft inhibiting the free propagation of the beam. Enhanced return currents can be attained through a tethered configuration, particularly if the passive (daughter) payload is biased positively, but plasma depletion and strong spacecraft charging still occur, albeit at later times. Increasing the speed of the spacecraft so that it moves through the plasma supersonically can further aid return-current collection but there is enhanced turbulence associated with the cross-field motion of the injection point so that strong beam distortion still occurs. There is also additional acceleration of ions in the ram of the beam.

An alternate way to reduce the spacecraft charging is via the injection of neutrals which are subsequently ionized by energetic electrons. However, the actual characteristics of the beam-plasma interaction depends on the region in which the neutrals are injected. If they are injected into the beam region, then ionization is predominately produced directly by the beam electrons. The amount of spacecraft charging is then limited to

a relatively small positive value that is required to stop the net forward momentum of the secondary electrons. The main disadvantage with this method is that enhanced short wavelength turbulence is induced via interactions of the newly created plasma and newly injected beam particles and this turbulence can destroy the coherence of the beam.

Alternately, the neutrals can be injected from the daughter. In this case, additional plasma can be produced by vehicle-induced ionization. This ionization is further enhanced if the daughter is biased positively so that energy of the return current electrons exceeds ionization threshold. This method was shown to be able to provide sufficient return current to maintain the beam-emitting payload at low (even negative) potential with the beam being able to easily propagate into the plasma with minimal distortion.

ACKNOWLEDGEMENTS

This research was supported by NASA grants NAGW-2471 and NAGW-1936 and NSF grant ATM 91-96132 to Southwest Research Institute.

REFERENCES

- [1] R. A. Arnoldy, and J. R. Winckler, *J. Geophys. Res.*, **86**, 575 (1981).
- [2] J.R. Winckler, *J. Spacecr. Rockets*, **20**, 293, (1983).
- [3] J. R. Winckler, J. E. Steffen, P. R. Malcolm, K. N. Erickson, Y. Abe and R. L. Swanson, *J. Geophys. Res.*, **89**, 7565, (1984).
- [4] J. R. Winckler, Y. Abe and K. N. Erickson, *Ion Acceleration in the Magnetosphere and Ionosphere*, Geophysical Monograph 38, AGU, 191, (1986).
- [5] J. R. Winckler, et al., *EOS*, **70**, 657, 1989.
- [6] R. L. Swanson, J. E. Steffen and J. R. Winckler, *Planet. Space Sci.*, **34**, 411, (1986).
- [7] D. A. Gurnett, W. S. Kurth, J. T. Steinberg, P. M. Banks, R. I. Bush and W. J. Raitt, *Geophys. Res. Lett.*, **13**, 225, (1986).
- [8] S. D. Shawhan, G. B. Murphy, P. M. Banks, P. R. Williamson and W. J. Raitt, *Radio Sci.*, **19**, 471, (1984).
- [9] Taylor, W.W.L., T. Obayashi, N. Kawashima, S. Sasaki, M. Yanagisawa, J.L. Burch, D.L. Reasoner and W.T. Roberts, *Radio Sci.*, **20**, 486, (1985).
- [10] T. Obayashi, and 12 others, *Earth Orient. Applic. Space Technol.*, **5**, 37, (1985).
- [11] S. Sasaki, N. Kawashima, K. Kuriki, M. Yanagisawa, and T. Obayashi, *J. Spacecr. Rockets*, **23**, 129, 1986.
- [12] P. M. Banks, and W. J. Raitt, *J. Geophys. Res.*, **93**, 5811 (1988).

- [13] P. M. Banks, W. J. Raitt, A. B. White, R. I. Bush, and P. R. Williamson, *J. Spacecr. Rockets*, **24**, 138, (1987).
- [14] B. N. Maehlum, J. Troim, N. C. Maynard, W. F. Denig, M. Friedrich, and K. M. Torkar, *Geophys. Res. Lett.*, **15**, 725 (1988).
- [15] W. F. Denig, N. C. Maynard, W. J. Burke and B. N. Maehlum, *J. Geophys. Res.*, **96**, 3601 (1991).
- [16] W. J. Raitt, P. R. Williamson, P. M. Banks, N. B. Myers and N. Kawashima, *Proc. of the 14th International Symposium on Space Tech. and Science*, 1501, (1984).
- [17] Sasaki, S., K-I. Oyama, N. Kawashima, W. J. Raitt and N. B. Myers, *EOS*, **67**, 1170, (1986).
- [18] B. E. Gilchrist, P. M. banks, T. Neubert, P. R. Williamson, N. N. Myers, W. J. Raitt, and S. Sasaki, *J. Geophys. Res.*, **95**, 2469 (1990).
- [19] T. Neubert and P. M. Banks, "Recent results from studies of electron beam phenomena in space plasmas", *Planet. Space Sci.*, submitted (1991).
- [20] R. M. Winglee, and P. J. Kellogg, *J. Geophys. Res.*, **95**, 6167, (1990).
- [21] R. M. Winglee, *J. Geophys. Res.*, **95**, 6191, (1990).
- [22] R. M. Winglee, and P.L. Pritchett, *J. Geophys. Res.*, **93**, 5823, (1988).

APPENDIX C

**Parameter Study of Radial Expansion of an Electron Beam
Injected into an ionospheric Plasma**

A Simulation Study of Radial Expansion of an Electron Beam Injected into an Ionospheric Plasma

J. Koga and C. S. Lin[†]
Department of Space Sciences
Southwest Research Institute
San Antonio, TX 78228

Abstract

Injections of nonrelativistic electron beams from a finite equipotential conductor into an ionospheric plasma have been simulated using a two-dimensional electrostatic particle code. The purpose of the study is to survey the simulation parameters for understanding the dependence of beam radius on physical variables. Due to low background plasma density, the conductor was charged to a higher potential. Beam electrons attracted by the charged conductor were decelerated to zero velocity near the stagnation point which is usually a few Debye lengths from the conductor. At the stagnation point, the beam electrons receive a large transverse kick and the beam expands radially. The beam electron buildup at the stagnation point produces a large electrostatic force responsible for the transverse kick. The simulations show that the electron beam radius for high spacecraft charging cases is of the order of the beam gyroradius, defined as the beam velocity divided by the gyrofrequency. The parameter survey indicates that the beam radius increases with beam density, and decreases with magnetic field and beam velocity. The beam radius normalized by the beam gyroradius is found to scale according to the ratio of the beam electron Debye length to the ambient electron Debye length. These results are useful for interpreting results of electron beam injection experiments conducted from rockets and the Space shuttle.

[†] Present address: Aurora Science Inc., San Antonio, TX 78228.

I. INTRODUCTION

Over the past 10 years many space and laboratory experiments have been devoted to the study of electron beams injected into an ionospheric plasma [Grandal, 1982; Kellogg *et al.*, 1982; Sasaki *et al.*, 1986; Banks *et al.*, 1987; Banks and Raitt, 1988]. The main objective of these experiments was to create auroral electron beams under controlled situations. The experiments examined beam propagation, wave emissions, instabilities, and other space plasma problems in the ionosphere [Grandal, 1982].

A variety of plasma waves are observed in the electron beam injection experiments [Gurnett *et al.*, 1986]. For plasma waves generated by a finite radius electron beam, both the wave generation mechanisms and instabilities are sensitively dependent on the beam density [Wong and Lin, 1990]. Since the beams are usually injected at a constant rate, the beam density is determined by the radial expansion. At constant injection rate, the density n varies as $n \propto r^{-2}$ where r is the beam radius. A small change in the beam radius would lead to large changes in the density. Therefore, the radius of an injection beam is a key parameter for understanding the plasma wave emissions observed during electron beam injection experiments.

Experimental observations of radial expansion have indicated that the beam can expand out to the electron beam gyroradius ρ_e , defined as the beam velocity v_b divided by the electron gyrofrequency Ω_e ($\rho_e = v_b/\Omega_e$) [Kellogg *et al.*, 1982]. Kellogg *et al.* [1982] studied radial expansion of electron beams injected into a background plasma and neutral gas. For cross field injections, the beam evolved into a hollow cylindrical shell structure of energetic electrons which propagated parallel to the local magnetic field. In cases where the electron gun was grounded, the envelope of beam was twice the beam electron gyroradius ρ_e for cross-field injection. For the aligned beam the radius of the envelope was $r_b \approx 0.25\rho_e$. In cases where the electron gun potential was allowed to float and no background plasma was present, the gun was surrounded by a luminous cloud with a radius approximately equal to the beam electron gyroradius. In these cases the gun potential rose to the electron beam accelerator potential. These early experiments suggested many factors which influence the radial expansion of the injected electron beams. Among these are the beam density, beam velocity, background plasma density, magnetic field strength, and the extent of spacecraft charging.

In early studies, analytic calculations [*Gendrin, 1974; Parks et al., 1975*] for electron beams injected parallel to magnetic field lines have shown that space charge effects play an important role during the initial phase of beam expansion. The calculations showed that magnetic field at the point of injection dictates the beam radius and beam density. However, the calculation did not take into account any possible beam instabilities or thermalization. Computer simulations of beam injection, which include these nonlinear effects, have thus been used in recent studies to examine the beam injection characteristics.

Computer simulations have demonstrated that spacecraft charging has a significant effect on the dynamics of the injected beam [*Okuda and Kan, 1987; Pritchett and Winglee, 1987; Winglee and Pritchett, 1987, 1988; Okuda and Bercham, 1988; Lin and Koga, 1989; Winglee, 1992; Koga and Lin, 1992*]. Where little or no charging occurs the beams easily propagated away [*Pritchett and Winglee, 1987; Winglee and Pritchett, 1988*]. In cases of charging to the beam energy most of the beam is stopped very close to the injection point [*Pritchett and Winglee, 1987; Winglee and Pritchett, 1987; Okuda and Bercham, 1988; Lin and Koga, 1989*]. The extent of the charging is attributed to many factors. The main factors determining the amount of the charging are n_b/n_0 , the ratio of the beam density n_b to the background density n_0 , and the background neutral density.

In particular, *Winglee and Pritchett*[1988] have simulated cross-field and parallel electron beam injection for parameters relevant to moderate spacecraft charging. For cross-field injection the beam is found to form a hollow cylinder of radius approximately equal to the beam gyroradius and width of about $2\lambda_{D_b}$ where $\lambda_{D_b} = v_b/\omega_b$. The thickness is attributed to repulsive forces associated with a net negative charge within the beam which causes it to expand radially. For parallel injection slower beam electrons are overtaken causing a net repulsive force which causes the beam to locally expand outward. The radius of cylinder is comparable to the cylindrical thickness in the cross-field injection case, much smaller than the beam gyroradius.

To study the electron beam radial expansion, we have used a two-dimensional electrostatic particle code to simulate the injection of electron beams from an finite equipotential conductor into a plasma [*Koga and Lin, 1992*]. Simulations are performed where beams are injected from

a finite equipotential conductor, which is charged to a high potential. The simulations were conducted for high beam current cases with beam density much greater than the ambient plasma density. The simulations indicate that charge buildup at the stagnation point causes the beam to expand radially to the beam electron gyroradius.

In this paper we present results from our simulation study of radial expansion characteristics of electron beams injected parallel to the magnetic field into an ionospheric plasma. Differing from the earlier study by [Winglee and Prichett, 1988], we concentrate on cases of high spacecraft charging which are more applicable to SEPAC electron beam firings. It is shown that radial expansion is significant. The objective of this paper is to examine physical parameters that determine the beam radial expansion. We performed a survey of simulation parameters to determine the dependence of beam radius on magnetic field, beam density and beam injection velocity. The effect of a neutral background is also examined. From the simulation, we suggested a mechanism to explain how beam drift velocity is transferred to the perpendicular direction. In the next section we will describe details of the simulation model. Section III presents the simulation results, and section IV discusses the results.

II. SIMULATION MODEL

Realistic modeling of beam injection from a spacecraft required injecting an electron beam from an isolated conductor. To study electron beam injection from an isolated conductor, we used a 2-D particle-in-cell code for the simulation geometry shown in Figure 1. The spacecraft is represented as a rectangle in the simulation box. In the electrostatic limit, the code treats the spacecraft boundary as an equipotential surface.

Particles are injected from the spacecraft surface in the simulation box every time step. The number of injected electrons per time step per cell is $N_c(e/q_e)(n_b/n_c)v_b\Delta t$, where N_c is the number of ambient electrons per cell, Δt is the simulation time step, n_b/n_c is the ratio of the beam density to ambient density, and e/q_e is the ratio of the ambient electron charge to the beam electron charge. The beam electrons have fractional charge and mass, which allows an increase in the number injected per time step. This larger number for the same beam density reduces numerical noise. These particles are placed in the simulation box at positions

$x = Rv_b\Delta t$ where x is the distance from the conductor surface, v_b is the injection velocity, and R is a random number between 0 and 1 for each injected particle. This method tends to fill in the fan between $x = 0$ and $x = v_b\Delta t$. The injected particles are randomly distributed across the beam in the y direction. All particles which strike the spacecraft surface are absorbed and their charge is accumulated.

Treating the spacecraft surface as a finite isolated equipotential conductor in an ambient plasma was accomplished by using the capacity matrix method [*Hockney and Eastwood*, 1981]. The capacity matrix relates the charge on each grid point on the spacecraft to the corresponding potential.

$$q_i = \sum_j C_{ij}\Phi_j \quad (1)$$

where C_{ij} is the capacity matrix, Φ_j is the spacecraft potential, and the sum j is over every grid point on the spacecraft. The capacity matrix is found by placing a unit charge on one point of the spacecraft surface with all other points zero and then solving for the potential. The values of the potential at each point on the spacecraft surface represent one column in the inverse capacity matrix $A = C^{-1}$. Repeating the process for each node then generates the full inverse matrix. The capacity matrix is obtained from the inverse of this matrix. This procedure is carried out only once at the beginning of the program. During the program the code first solves Poisson's equation for the electric potential Φ_0 with charge evenly distributed on the spacecraft surface. It next uses the capacity matrix of the conductor to redistribute the charge and maintain the spacecraft surface at an equipotential using the formulae:

$$\Delta q_i = \sum_j C_{ij}(\Phi_{eq} - \Phi_{0j}) \quad (2)$$

$$\Phi_{eq} = \sum_{ij} C_{ij} / \sum_{ij} C_{ij} \quad (3)$$

where Δq_i is the charge added to each grid point on the spacecraft. Using the redistributed charge density, the code again solves Poisson's equation for the electric potential of the spacecraft.

We use a periodic boundary condition for the lower boundary at $y = 0$ and the upper

boundary at $y = L_y$ where L_y is the simulation length in the y direction. The electrostatic potential at $x = 0$, $\phi(x = 0, y)$, is constant. We assume the potential is zero at the right boundary at $x = L_x$ where L_x is the simulation length in the x direction. The right boundary condition approximates the potential at infinity. In the simulation magnetic field is assumed to be uniform in the x direction.

Ambient ions and electrons are initialized uniformly in the system. Both the ambient ions and electrons have Maxwellian velocity distributions with the same temperature, $T_e = T_i$ where T_e and T_i are the electron and ion temperatures, respectively. At the right and left boundary, the code specularly reflects all particles.

III. SIMULATION RESULTS

The simulation uses a $512\Delta \times 128\Delta$ grid in the x and y directions, respectively. The spacecraft is represented by a rectangular box centered on $x = 102\Delta$ and $y = 64\Delta$ with size $4\Delta \times 32\Delta$ in the x and y directions, respectively. The grid size, Δ , equals the Debye length of the ambient electrons defined as $\lambda_d = a_c/\omega_{pe}$ where $a_c = (2T_e/m_e)^{1/2}$ is the thermal velocity of the ambient electrons and ω_{pe} is the ambient electron plasma frequency. We choose the ion to electron mass ratio to be 100, and $a_c = 0.001c$ where c is the speed of light, a unit of the simulation. We use a reference electron gyrofrequency Ω_{ce} of $0.25\omega_{pe}$, which is close to the ionospheric value of $0.3\omega_{pe}$. The simulations use a time step $\Delta t = 0.05\omega_{pe}^{-1}$ and 131,072 particles for the ambient plasma. For the reference case the electron beam has a width of 4Δ , an injection velocity of $v_b = 10a_c$ along the x axis, and zero initial thermal velocity.

We describe the simulation results on two cases of beam injection: weak charging with a density ratio of $n_b/n_c = 0.1$, and strong charging with $n_b/n_c = 10$.

Weak Charging Potential Simulations

The phase space and configuration space results for weak beam injection, $n_b/n_c = 0.1$, are shown in Figures 2a and 2b at time $\omega_{pe}t = 30$, respectively. The $x - v_x$ phase space plot shows that the beam is not withheld by the charging of the spacecraft. The beam electrons move near their injection velocity until approximately 40Δ from the injection point. After

this point the beam-plasma instability occurs from approximately 40Δ to 400Δ from the beam injection point. The wavelength of the instability corresponds to approximately 50Δ which is close to the wavelength of 60Δ predicted from linear theory. Figure 3 shows that the spacecraft potential oscillates about zero and the maximum amplitude of the potential energy is $e\phi/E_b \approx 0.04$ where E_b is the beam energy. Therefore there is very little charging of the spacecraft. From the $x - y$ configuration space plot in Figure 2b it is apparent that the beam remains at its initial beam width until the onset of the instability and expands radially after the onset. A contour plot of the beam density delineates the beam edge in Figure 4a. The lowest contour level is chosen to be $n_b/n_0 = 0.001$ where n_b is the beam density and n_0 is the normalization density. So it separates the region with no beam particles from the regions containing beam particles. The beam radius measured from the contour plot is $r_b/\rho_e \approx .32$ where $\rho_e = v_b/\Omega_{ce}$ is the beam electron and v_b is the initial beam velocity. In Figure 4b the density profile along the center of the beam is shown. It is apparent that the maximum radial expansion occurs where the beam density is a minimum. The minimum expansion occurs where the density is a maximum.

Strong Charging Potential Simulations

Figures 5 and 6 show results of electron beam injection for the the high charging case where $n_b/n_0 = 10$. The phase space plot $x - v_x$ at $\omega_{pe}t = 30$ in Figure 5a indicates that the point at which beam electrons are stopped (stagnation point) is very close to the conductor surface. Due to the high beam density the spacecraft becomes positively charged, causing the beam electrons to be rapidly drawn back to the spacecraft surface. Figure 5b, the $x - y$ plot at time $\omega_{pe}t = 30$, shows that some returning beam electrons overshoot the spacecraft and are drawn back on the wake side.

The electrostatic potential of the spacecraft is observed to rise rapidly to $\approx 94\%$ of the beam energy within $\omega_{pe}t < 3$. The potential then oscillates around this value till the end of the run. Some electrons at the front of the beam are accelerated along the magnetic field to velocities higher than the original beam velocity. The maximum velocity v_{max} is approximately $1.5v_b$ where v_b is the initial beam velocity. This acceleration of beam particles to velocities higher

than the initial beam velocity is due to the bunching of beam electrons behind the beam head.

Figure 5b indicates that the electron beam expands radially. A contour plot of the beam density delineates the beam edge in Figure 6a. The lowest contour level is chosen to be $n_b/n_0 = 0.001$, the same as Figure 4a. So it separates the region with no beam particles from the regions containing beam particles. The contour lines near the spacecraft injection point indicate a region where the beam density is higher than the initial injection density $n_b/n_0 > 10$. The highest beam density is at the stagnation point of the beam (Figure 6b). The beam radius measured from the contour plot is $r_b \approx \rho_e$. In $x - y$ plots at $\omega_{pe}t = 10$ and $\omega_{pe}t = 20$ the maximum beam expansion also occurs very close to the spacecraft surface near the stagnation point.

Figures 7a and 7b show that the maximum transverse electric field E_y and the maximum longitudinal electric field E_x occur at where the beam density is highest. The transverse velocities to which the beam electrons are accelerated depend on the time spent in the stagnation region, where the transverse electric field E_y is large. An estimate of the acceleration time can be obtained from the width of the transverse electric field region and the initial beam velocity. Using the value of approximately 8Δ for the width it is apparent that the beam particles can be accelerated to $.75v_b$ where v_b is the initial beam velocity. In general beam electrons travel through the stagnation region with velocities lower than the initial beam velocity. So they spend more time in the stagnation region and are accelerated to higher velocities.

After the stagnation region, the transverse electric field E_y is smaller (Figure 7a) and the average beam velocity is higher (Figure 5a). E_y drops off very quickly after the stagnation region. Within a few grid cells E_y drops by a factor of 3 (Figure 7a). Therefore, the beam electrons receive their largest transverse kick very close to the spacecraft and experience smaller transverse impulses from that point. The large E_y between $x = 128\Delta$ and $x = 256\Delta$ is caused by the beam electrons bunching in y from the gyromotion. This can be seen in the $x - y$ plot in Figure 5b where the beam narrows in y .

In the next sections we examine the variation of the maximum radial expansion distance with magnetic field, beam density, beam velocity, and neutral density for the case of high charging .

Variation with Magnetic Field Strength

Figure 8 shows beam density plots at $\omega_{pe}t = 30$ where the contour lines indicate the beam envelope. In this figure, we vary the magnetic field while keeping all other parameters the same as Figure 5. The ratio Ω_{ce}/ω_{pe} is 0.25, 0.5, and 1.0 down the page with all other parameters fixed. As in the case of Figure 5, the conductor is charged to high potential. Note that the maximum beam radius decreases with increasing magnetic field. However, the ratio of the maximum beam radius to the electron gyroradius r_b/ρ_e is approximately 1 for each of these cases. This indicates that in the range of ionospheric magnetic field values the beam electrons receive the same transverse kick and expand to ρ_e when charging is significant. In Figure 8c, where $\Omega_{ce}/\omega_{pe} = 1.0$, no beam electrons are in the wake region of the spacecraft. The maximum width beam electrons achieve, $2r_b$, is smaller than the spacecraft width. So all returning beam electrons strike the spacecraft surface.

Variation with Beam Density

We ran a series of simulations by varying the beam to ambient plasma density ratio n_b/n_c from 1 to 20 for the cases of $\Omega_{ce}/\omega_{pe} = 0.25$ (solid line) and 0.5 (dotted line). The maximum value of the ratio of r_b/ρ_e for each run is plotted as a function of n_b/n_c in Figure 9. The ratio r_b/ρ_e is between 0.725 for $n_b/n_c = 1$ and 1.3 for $n_b/n_c = 20$. The ratio r_b/ρ_e gradually increases with beam density. This indicates that the transverse kick of the beam electrons gradually increases with beam density.

The relative magnitude of the transverse kick can be inferred from the average velocity of the beam electrons through the stagnation region. The average velocity determines roughly the time that the beam electrons are accelerated by the transverse electric fields E_y in the stagnation region. Figure 10 shows the average velocity of beam electrons at the stagnation point versus beam density for $\Omega_{ce}/\omega_{pe} = 0.25$ (solid line) and 0.5 (dotted line) at $\omega_{pe}t = 30$. The velocity is averaged across the beam and the stagnation point is taken to be the point where the longitudinal electric field E_x is a maximum. The average velocity decreases with increasing beam density for both values of magnetic field (Figure 10). Therefore, beam elec-

trons spend more time in the stagnation region for higher density beams and are accelerated to higher transverse velocities.

This velocity trend can be understood from the ratio of the electron beam Debye length $\lambda_{Db} = v_b/\omega_b$ to the ambient electron Debye length λ_d :

$$\frac{\lambda_{Db}}{\lambda_d} = \left(\frac{v_b}{a_c}\right)\left(\frac{n_c}{n_b}\right)^{1/2}, \quad (4)$$

The electron beam Debye length λ_{Db} represents the charge separation distance between the spacecraft and the beam stagnation point. The ambient electron Debye length λ_d indicates the distance that ambient electrons neutralize excess charge. As λ_{Db}/λ_d decreases the beam electrons feel more the electrostatic potential of the spacecraft since ambient electrons have a harder time shielding the effects of the retarding potential drop. Therefore, the beam electrons travel with lower velocities. This ratio decreases with increasing beam density n_b as $n_b^{-1/2}$ following the trend of the average velocity in Figure 10.

Variation with Beam Velocity

Figure 11 shows the beam radius normalized to the electron gyroradius r_b/ρ_e as a function of initial injection velocity v_b at $\omega_{pe}t = 30$. The injection velocity v_b/a_c normalized by a_c , the ambient electron thermal velocity, was varied between 2.5 and 20 in the simulation runs. All other parameters were kept the same as in the reference case (Figure 5). The radial expansion is largest for small velocity injection and *vice versa*. The relative magnitude of the transverse kick can again be inferred from the average velocity of the beam electrons through the stagnation region. Figure 12 shows the average velocity of beam electrons at the stagnation point versus initial beam injection velocity at $\omega_{pe}t = 30$. The average velocity increases with the initial beam injection velocity. Beam electrons spend more time in the stagnation region for lower injection velocities and are, therefore, accelerated to higher relative transverse velocities. This velocity trend can also be interpreted from the ratio λ_{Db}/λ_d in Equation 4, which increases linearly with the initial beam injection velocity. As the beam injection velocity increases, the ambient electrons more easily shield excess charge buildup over the beam electron Debye length. Therefore, the beam electrons travel with higher velocities

through the stagnation region, which is in agreement with Figure 12.

IV. DISCUSSION

We have examined the radial expansion properties of a nonrelativistic electron beam injected along magnetic field lines into a background plasma. The simulations show that the beam radius after expansion is proportional to the beam gyroradius. In our reference case with $n_b/n_c = 10$ and $v_b/a_c = 10$, the beam radius after expansion is approximately equal to the beam electron gyroradius ρ_b . To further determine the dependence of beam radius on other plasma variables, we conducted a parameter survey of high beam current cases where spacecraft charging is significant. The survey indicates that the beam radius normalized by beam gyroradius increases with beam density and decreases with beam injection velocity.

Strong Spacecraft Charging

The parameter survey results presented in this paper are most applicable to electron beam injection experiments that produce high spacecraft charging potential. The spacecraft potential energy varied between 60% and 100% of the beam energy when the beam to ambient plasma density ratio n_b/n_c varies from 1 to 20. It is shown that radial expansion is significant.

In satellites and the shuttle charging up to the beam energy is often observed [*Sasaki et al.*, 1986]. Space Experiments with Particle Accelerators (SEPAC) during the Spacelab 1 mission indicated that the electron beam injection had charged the spacecraft to a potential as high as the beam energy, which was 5 keV [*Sasaki et al.*, 1986]. Because the ambient plasma cannot neutralize the electron beam and the spacecraft, the net beam charge and the spacecraft charging are important in this case in determining beam propagation and expansion.

In the case of high spacecraft charging, spacecraft charging is responsible for the radial expansion of the electron beam. Beam particles are stopped by the charged spacecraft very close to the spacecraft surface at the stagnation point. At this point the density is highest due to conservation of flux. The highest beam density is at the stagnation point of the beam (Figure 5b) which is in agreement with analytical results for one-dimensional electron beam injection into a vacuum [*Parks et al.*, 1975]. Physically, the high density at the stagnation

point is a result of the approximate conservation of flux $n_b v_b$. At the stagnation point, where the average beam velocity v_b is smallest, the density n_b should be highest assuming substantial expansion of the beam has not occurred.

The simulations suggest that the beam electrons expand because they receive a large transverse kick at the stagnation point. This kick, which occurs very close to the injection point, determines the beam envelope from that point on. The transverse kick is produced by electrostatic force due to charge build up at the stagnation points as the beam electrons slow down.

The dependence of the injected electron beam radius on the beam density and the injection velocity can be understood from the average velocity of the beam electrons passing through the stagnation point. The average velocity indicates the time beam electrons spend in the stagnation region and, therefore, how long beam electrons are accelerated by the transverse electric fields. As Figure 10 shows, the average beam velocity in the stagnation region decreases with the beam density. The final transverse velocity of the beam electrons and, thus, the beam envelope increases with beam density. Similarly, the average velocity of beam electrons through the stagnation region increases with beam injection velocity (Figure 12). Therefore, beam electrons with high injection velocity are accelerated to lower relative transverse velocities than beam electrons with low injection velocities.

The ratio of λ_{Db}/λ_d , which is an indication of how well beam electrons are shielded from the charged spacecraft surface by the ambient electrons, can also be used to explain the dependence of beam radius on beam density and beam injection velocity. This dependence is evident from Figure 10 where the average beam velocity at the stagnation point drops off approximately as $n_b^{-1/2}$ and from Figure 12 where the average velocity increases almost linearly with beam injection velocity v_b .

Weak Spacecraft Charging

The simulations indicate that without charging, the injected electron beam is expanded slightly. However, the reason for expansion is different from the strong charging cases. In the case of very little charging of the spacecraft (Figure 2-3), the beam remains at its initial

width until the onset of the beam-plasma instability and expands radially after the onset. In Figure 4b the density profile along the center of the beam is shown. It is apparent that the maximum radial expansion occurs where the beam density is a minimum, and the opposite is true. It appears that the beam-plasma instability excites the expansion of the beam. The beam-plasma instability causes the characteristic oscillations of beam particles in the $x - v_x$ phase space (Figure 2a). Some particles are slowed and some are accelerated. When the beam particles are slowed by the instability, there is a density buildup from conservation of flux. This density buildup results in a large radial component of the electric field which causes the beam to expand. It appears that once this motion is excited the beam continues to expand and contract radially.

In all the experiments the injected beams charged the spacecraft to a range of levels. In the case of rockets very little charging is observed [Maehlum, 1988]. A high density neutral background is present at the low altitudes which the rockets fly. The beams ionize the neutrals and generate secondary electrons and ions which neutralize the spacecraft. This allows the beam to propagate away. According to our simulation results, the injected electron beam from a rocket would have a small beam radius determined mainly by beam plasma instabilities.

In the Vehicle Charging and Potential (VCAP) experiment on the Space Shuttle Orbiter mission STS-3 camera images show narrow collimation of an electron beam fired transverse to the magnetic field for a short distance before appreciable beam spreading seems to occur [Banks *et al.*, 1987; Banks and Raitt, 1988]. At the point of spreading an abrupt decrease in the light emission of the electron beam is observed. Various interpretations have been suggested; The abrupt decrease in light emission could be a manifestation of electrostatic beam spreading caused by the negative charge density of the beam, beam electrons undergoing intense scattering in an electrostatic wave field associated with instabilities, or an excess luminosity effect associated with the penetration of the electron beam through a boundary layer of vehicle-associated outgassing products.

Because the vehicle electric potential induced by these electron beam firings was normally a few volts to a few tens of volts with a beam energy of 1 keV [Banks *et al.*, 1987], the experiment parameters and conditions are more comparable to the weak charging cases shown in Figures

2-4. The weak charging simulations show similar characteristics as the VCAP experiment results: narrow beam collimation and beam propagation before the beam spreading. We would then argue that the beam spreading is caused by the charge density perturbation of beam plasma instabilities.

Effects of Neutral Gas

In the environment surrounding rockets and the Space shuttle in the ionosphere, the neutral gas density could be sufficiently high to have large effects on spacecraft charging. It is known that neutral gas around the spacecraft reduces charging. We thus here briefly discuss the effects of neutral gas on radial expansion. We conducted simulations with a neutral background. The simulation had parameters the same as the high charging case. The neutral background occupies a region which starts at the left boundary of the simulation $x = 0$ and ends at $x = x_i + 16\Delta$ beyond the injection point x_i . This finite region takes into account the cloud of neutrals which generally surround spacecraft either from outgassing or neutral gas injection. The density of the neutrals is chosen to be 10^{13} cm^{-3} .

The simulation with the neutral background indicates that the stagnation point is farther from the conductor surface than without the neutrals and the electron beam expands radially. The radial expansion of the beam is slightly reduced from the injection without the neutrals. The beam radius measured from the contour plot indicates that $r_b \approx 0.84\rho_e$ at $\omega_{pe}t = 30$.

The simulation shows that the radial expansion of the beam is reduced for beam injection into a plasma and neutral gas. This reduction can be mainly attributed to the reduction of spacecraft charging by the influx of secondary electrons produced near the spacecraft surface. The $x - y$ plots at time $\omega_{pe}t = 30$ in Figures 13a and 13b show the secondary electrons and ions produced near the spacecraft. The neutrals are ionized by the electron beam near the spacecraft surface and by background plasma electrons accelerated towards the positively charged spacecraft. The secondary electrons are responsible for reducing spacecraft charging. The generation of secondaries near the spacecraft increases the ambient electron Debye length λ_d . The charge build up near the stagnation point is more easily neutralized. Therefore the transverse electric field is smaller and the beam electrons travel through the stagnation point

with higher velocities. The net effect is less expansion of the beam.

Summary

The simulations have been conducted to study systematically the radial expansion of an injected electron beam into the ionosphere. The radial expansion mechanism is examined. In addition, the dependence of beam radius on magnetic field, density and beam velocity is determined. The beam radius dependence is critically needed for understanding the phenomena of beam propagation and wave emissions associated with the beam injection experiments. Plasma instability conditions usually depend on beam density, which is in turned determined by the beam radius for constant beam current injections. The radial expansion of electron beams injected into the ionosphere is found to be closely related to the amount of spacecraft charging. While little or no charging occurs, the beam propagates away with a slight radial expansion. In case of appreciable spacecraft charging, the injected electron beam expands immediately after beam electrons pass through the stagnation point. The radial expansion is caused by strong electrostatic repulsive forces due to charge buildup at charge build up at the stagnation point. These simulation results can be used for interpreting measurements of active beam experiments.

ACKNOWLEDGMENTS

We would like to thank R. M. Winglee for many useful suggestions on techniques of simulating beam injection. The work was supported by NASA contract NAGW-1296. The particle simulations were performed on the CRAY-YMP at NASA Goddard Space Flight Center.

REFERENCES

- Banks, P. M., W. J. Raitt, A. B. White, R. I. Bush, and P. R. Williamson, Results from the vehicle charging and potential experiment on STS-3, *J. Spacecr. Rockets*, 24, 138, 1987.
- Banks, P. M. and W. J. Raitt, Observations of electron beam structure in space experiments, *J. Geophys. Res.*, 93, 5811, 1988.
- Gendrin, R., Initial expansion phase of artificially injected electron beam, *Planet. Space Sci.*, 22, 633, 1974.

- Grandal, B., ed., *Artificial Particle Beams in Space Plasma Studies*, Plenum, New York, 1982.
- Gurnett, D. A., W. S. Kurth, J. T. Steinberg, P. M. Banks, R. I. Bush, and W. J. Raitt, Whistler-mode radiation from the Spacelab-2 electron beam, *Geophys. Res. Lett.*, 13, 225, 1986.
- Hockney, R. W. and J. W. Eastwood, *Computer simulation using particles*, McGraw-Hill, New York, 1981.
- Kellogg, P. J., H. R. Anderson, W. Bernstein, T. J. Hallinan, H. R. Holzworth, R. J. Jost, H. Leinbach, and E. P. Szuszuczewicz, Laboratory simulation of injection particle beams in the ionosphere, in *Artificial Particle Beams in Space Plasma Studies*, edited by Bjorn Grandel, pp. 289-329, Plenum, New York, 1982.
- Koga, J. K. and C. S. Lin, Simulations of radial expansion of an injected electron beam, in *Physics of Space Plasmas (1991)*, edited by T. Chang, G. B. Crew, and J. R. Jasperse, pp. 405-410, Scientific Publishers, Inc., Cambridge, Mass., 1992.
- Lin, C. S. and J. K. Koga, Spacecraft charging potential during electron-beam injections into space plasmas, *IEEE Trans. Plasma Sci.*, 17, 205, 1989.
- Maehlum, B. N., Beam-plasma experiments, *Computer Phys. Commun.*, 49, 119, 1988.
- Okuda, H. and J. R. Kan, Injection of an electron beam into a plasma and spacecraft charging, *Phys. Fluids*, 30, 209, 1987.
- Okuda, H. and J. Berchem, Injection and propagation of a nonrelativistic electron beam and spacecraft charging, *J. Geophys. Res.*, 93, 175, 1988.
- Omura, Y. and H. Matsumoto, Computer simulations of beam injection experiments for SEPAC/Spacelab 1 mission, *Radio Sci.*, 19, 496, 1984.
- Parks, D. E., A. R. Wilson, and I. Katz, Monode plasma sheath dynamics, *IEEE trans. Nucl. Sci.*, NS-22, 2368, 1975.
- Pritchett, P. L. and R. M. Winglee, The plasma environment during particle beam injection into space plasmas, 1, electron beams, *J. Geophys. Res.*, 92, 7673, 1987.
- Sasaki, S., N. Kawashima, K. Kuriki, M. Yanagisawa, and T. Obayashi, Vehicle charging observed in SEPAC Spacelab-1 experiment, *J. Spacecr. Rockets*, 23, 129, 1986.

Winglee, R. M. and P. L. Pritchett, Space charge effects during the injection of dense electron beams into space plasmas, *J. Geophys. Res.*, 92, 6114, 1987.

Winglee, R. M. and P. L. Pritchett, Comparative study of cross-field and field-aligned electron beams in active experiments, *J. Geophys. Res.*, 93, 5823, 1988.

Winglee, R. M., Simulations of the active injection of electron beams, *Physics of Space Plasmas (1991)*, edited by T. Chang, G. B. Crew, and J. R. Jasperse, pp. 349-362, Scientific Publishers, Inc., Cambridge, Mass., 1992.

Wong, H. K. and C. S. Lin, Plasma instabilities of a finite-radius electron beam in a uniform plasma, *Radio Science*, 25, 277, 1990.

FIGURE CAPTIONS

- Fig. 1. Configuration of the simulation system. The shaded rectangle represents the spacecraft. Electron beam injection and magnetic field directions are in the $+x$ direction.
- Fig. 2. Phase space plots of weak charging simulations with $n_b/n_c = 0.1$ and $v_b/a_c = 10$ at $\omega_{pe}t = 30$. (a) The beam electron phase space in the $x-v_x$ plane and (b) the positions of beam electrons in the $x-y$ plane. The position is normalized by the Debye length and the velocity is normalized by the initial beam injection velocity.
- Fig. 3. Spacecraft potential as a function of time step.
- Fig. 4. Density plots of beam electrons at $\omega_{pe}t = 30$ for $n_b/n_c = 0.1$ and $v_b/a_c = 10$. (a) Contour lines delineate the envelop of beam electrons (b) Profile of beam density along beam showing maximum density at about 128Δ from the conductor.
- Fig. 5. Phase space plots of beam electrons at $\omega_{pe}t = 30$ for the case of strong charging potential, (a) the beam electron phase space in the $x-v_x$ plane and (b) the positions of beam electrons in the $x-y$ plane. The simulation parameters are $n_b/n_c = 10$ and $v_b/a_c = 10$.
- Fig. 6. (a) Contour plot of beam electron density (top panel) and (b) profile of beam density (bottom panel) averaged over y at the end of the simulation ($\omega_{pe}t = 30$). The parameters are $n_b/n_c = 10$ and $v_b/a_c = 10$. Profile of beam density along the beam (bottom panel) shows that the maximum density is close to spacecraft surface. The outer contour line delineates the beam envelope and the small shaded area has more than 10 beam electrons per cell. The vertical slit near the shaded contour line represents the conductor. (b) profile of the beam density
- Fig. 7. Profiles of maximum field quantities E_y and E_x across the beam versus the x coordinate at $\omega_{pe}t = 30$ for the simulation shown in Figure 5. The top panel presents (a) the maximum transverse electric field E_y , and the bottom panel presents (b) the maximum longitudinal electric field E_x across the y coordinate. Profiles of the maximum transverse electric field (top) and the maximum longitudinal electric field (bottom). The maximum values are determined from a column of cells at each given x position.
- Fig. 8. Density contour plots of beam electrons at $\omega_{pe}t = 30$ for $n_b/n_c = 10$ and $v_b/a_c = 10$. Contour lines delineate the beam envelope for (a) $\Omega_{ce}/\omega_{pe} = 0.25$, (b) 0.5, and (c) 1.0

Fig. 9. Electron beam envelope radius r_b/ρ_e versus n_b/n_c at $\omega_{pe} = 30$ for $v_b/a_c = 10$.

Fig. 10. Average velocity v_x at the stagnation point normalized to ambient electron thermal velocity a_c versus n_b/n_c at $\omega_{pe} = 30$ for $v_b/a_c = 10$.

Fig. 11. Electron beam envelope radius r_b/ρ_e versus the beam injection velocity v_b/a_c at $\omega_{pe} = 30$ for $n_b/n_c = 10$.

Fig. 12. Absolute value of average velocity v_x at the stagnation point normalized to ambient electron thermal velocity a_c versus initial injection velocity v_b/a_c at $\omega_{pe} = 30$ for $n_b/n_c = 10$.

Fig. 13. Configuration plots of (a) secondary electrons and (b) secondary ions in the $x - y$ plane for the simulation of electron beam injected into a background of ambient plasma with neutral gas. The plasma parameters are the same as the high charging case (Figure 5), $n_b/n_c = 10$ and $v_b/a_c = 10$.

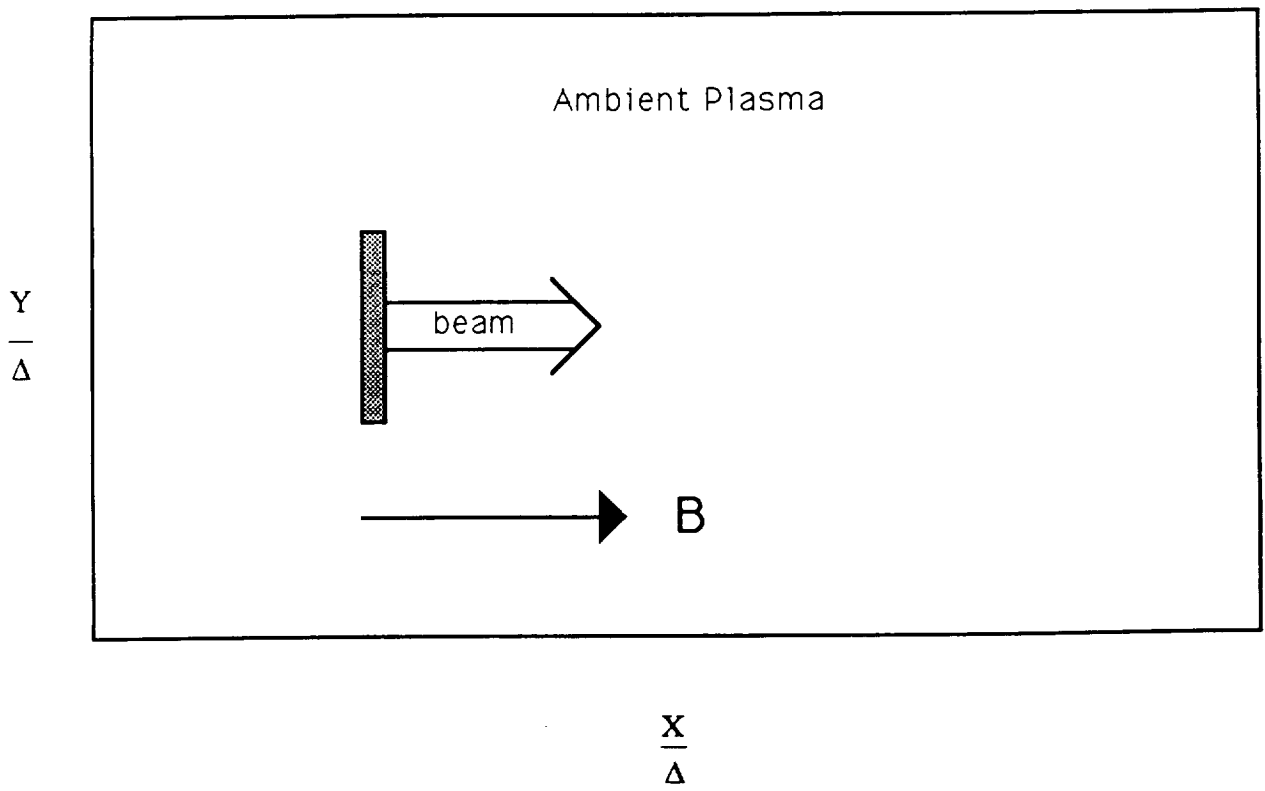


Figure 1

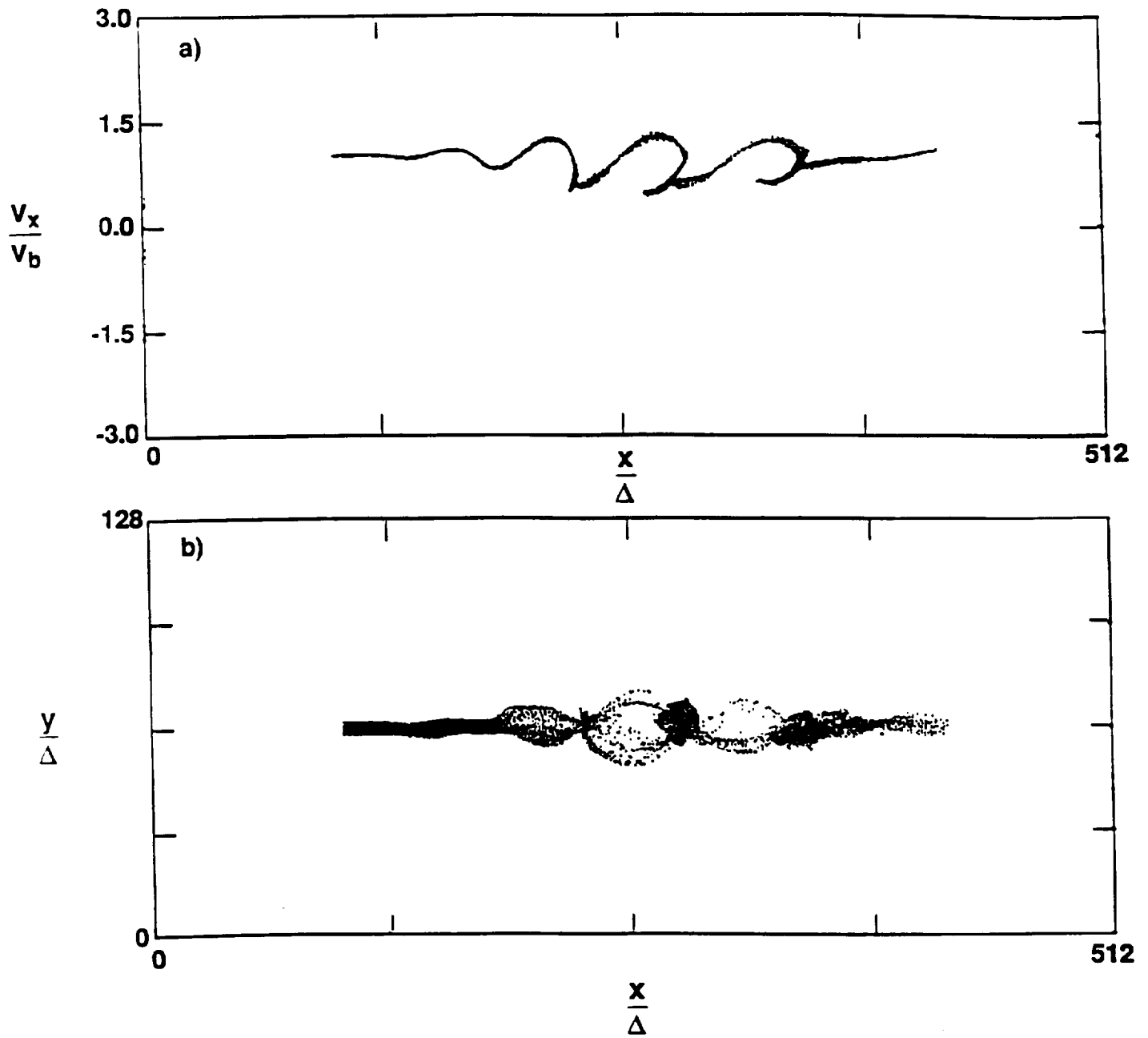


Figure 2

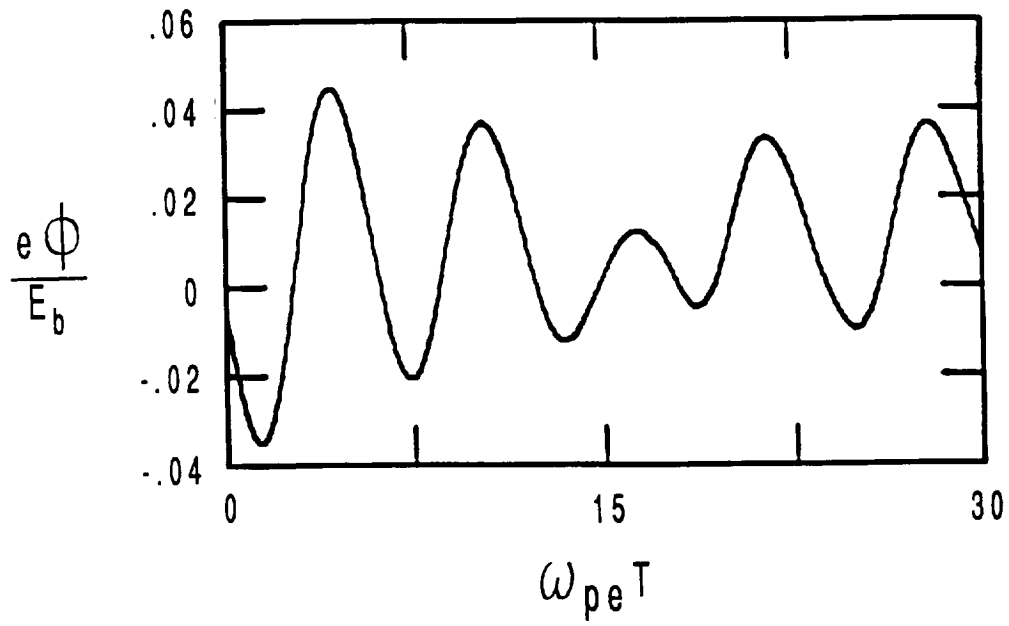


Figure 3

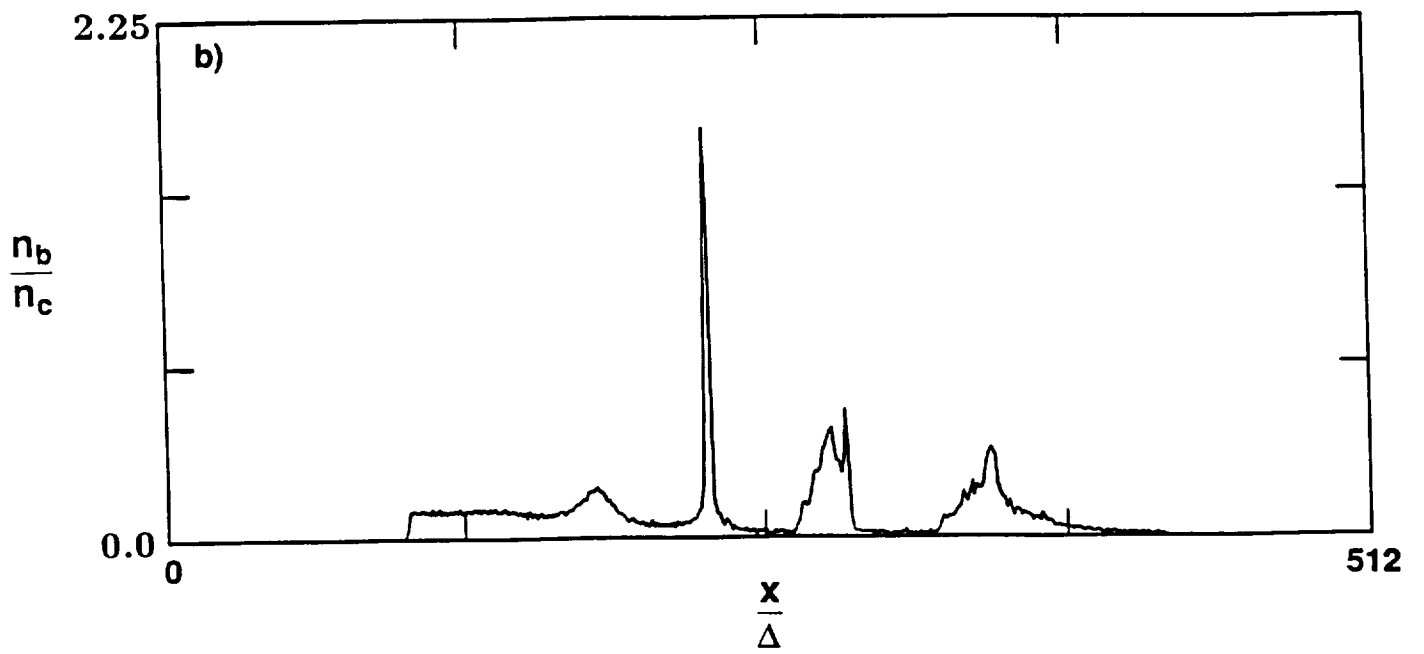
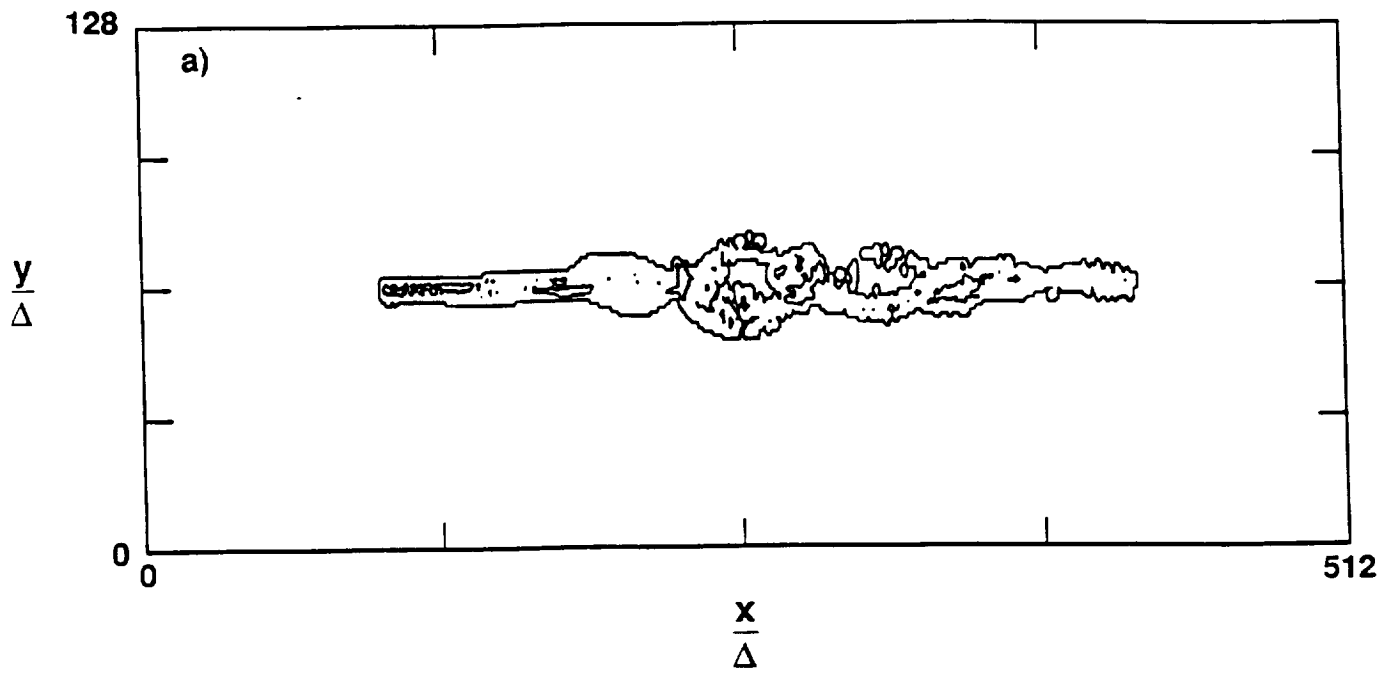


Figure 4

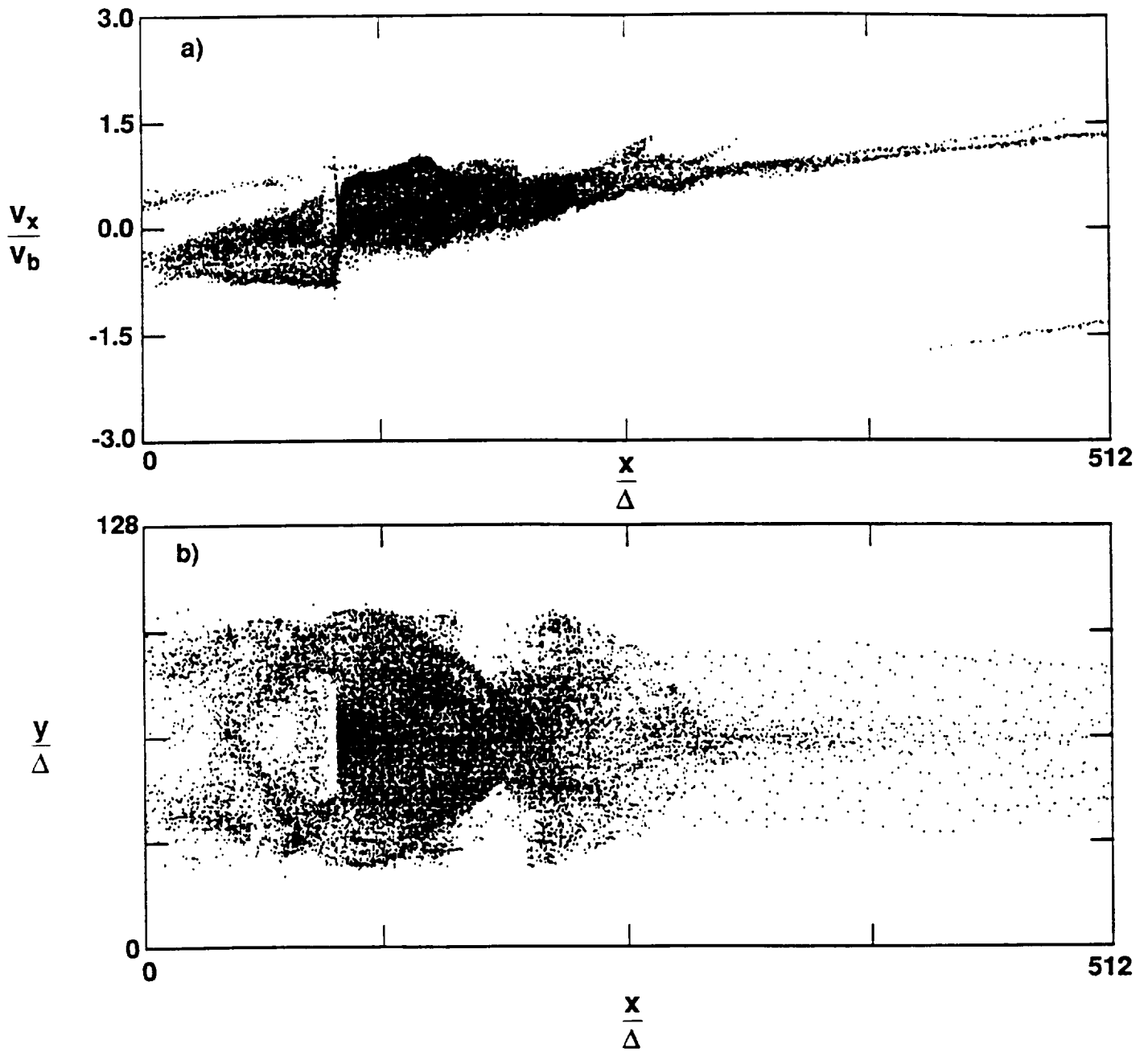


Figure 5

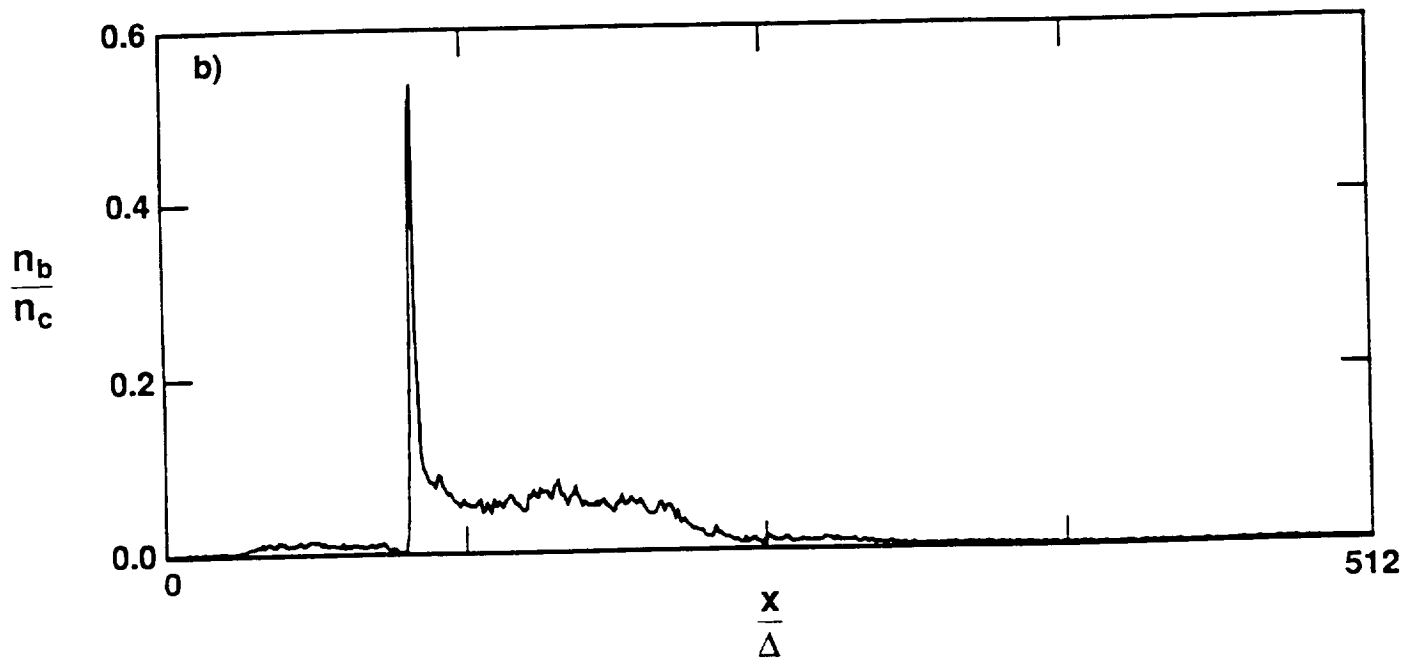
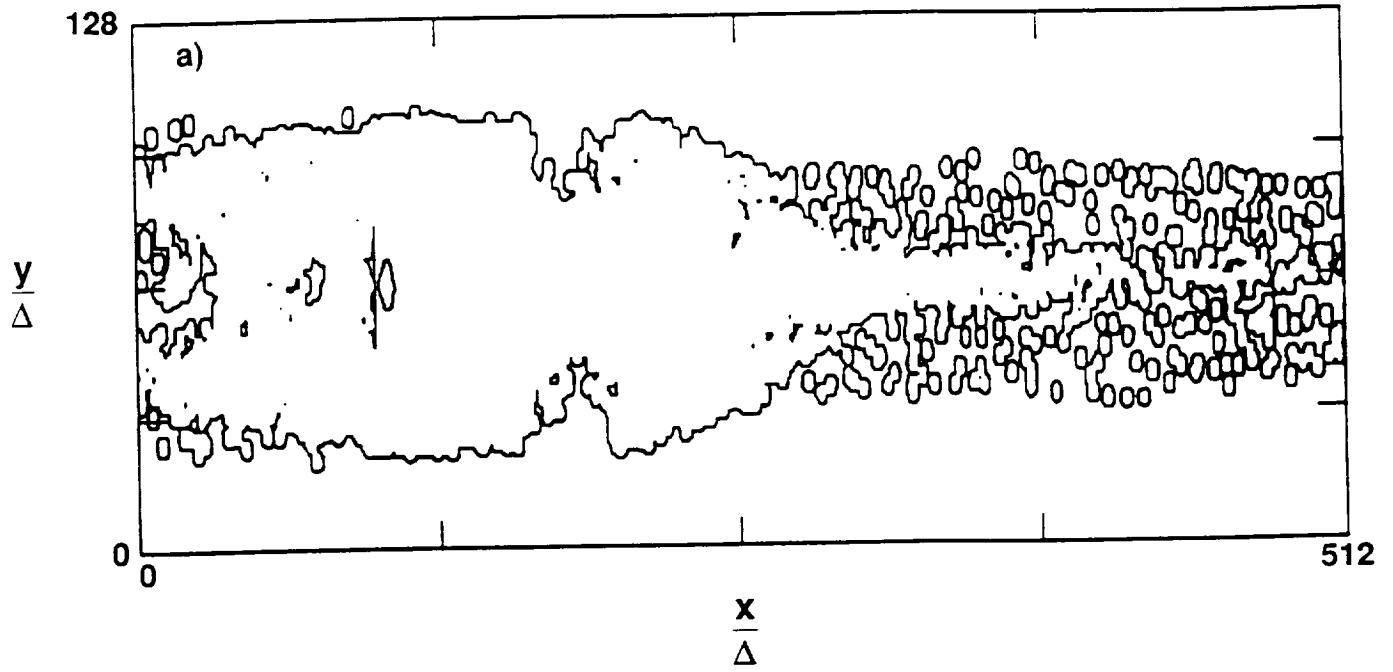


Figure 6

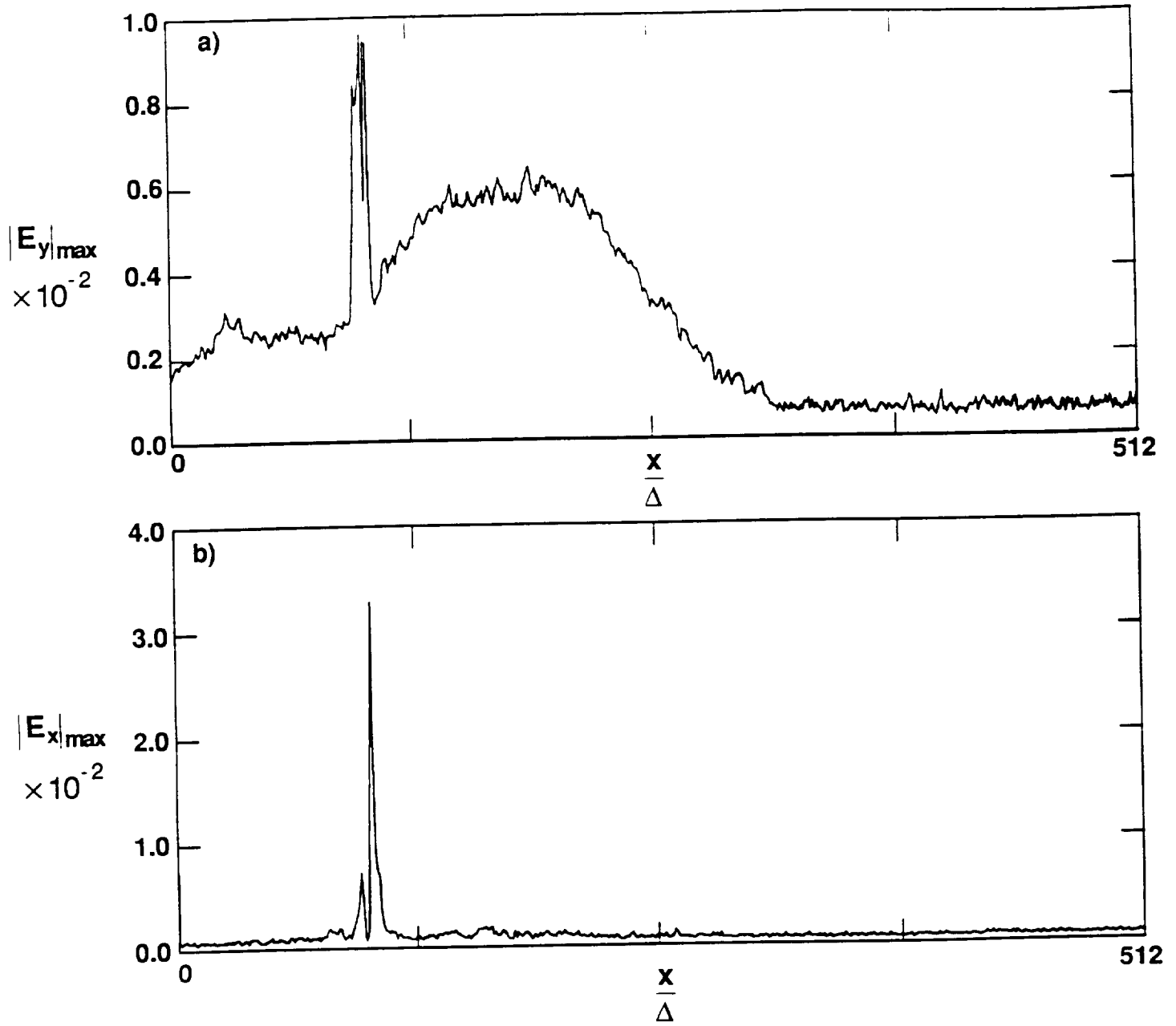


Figure 7

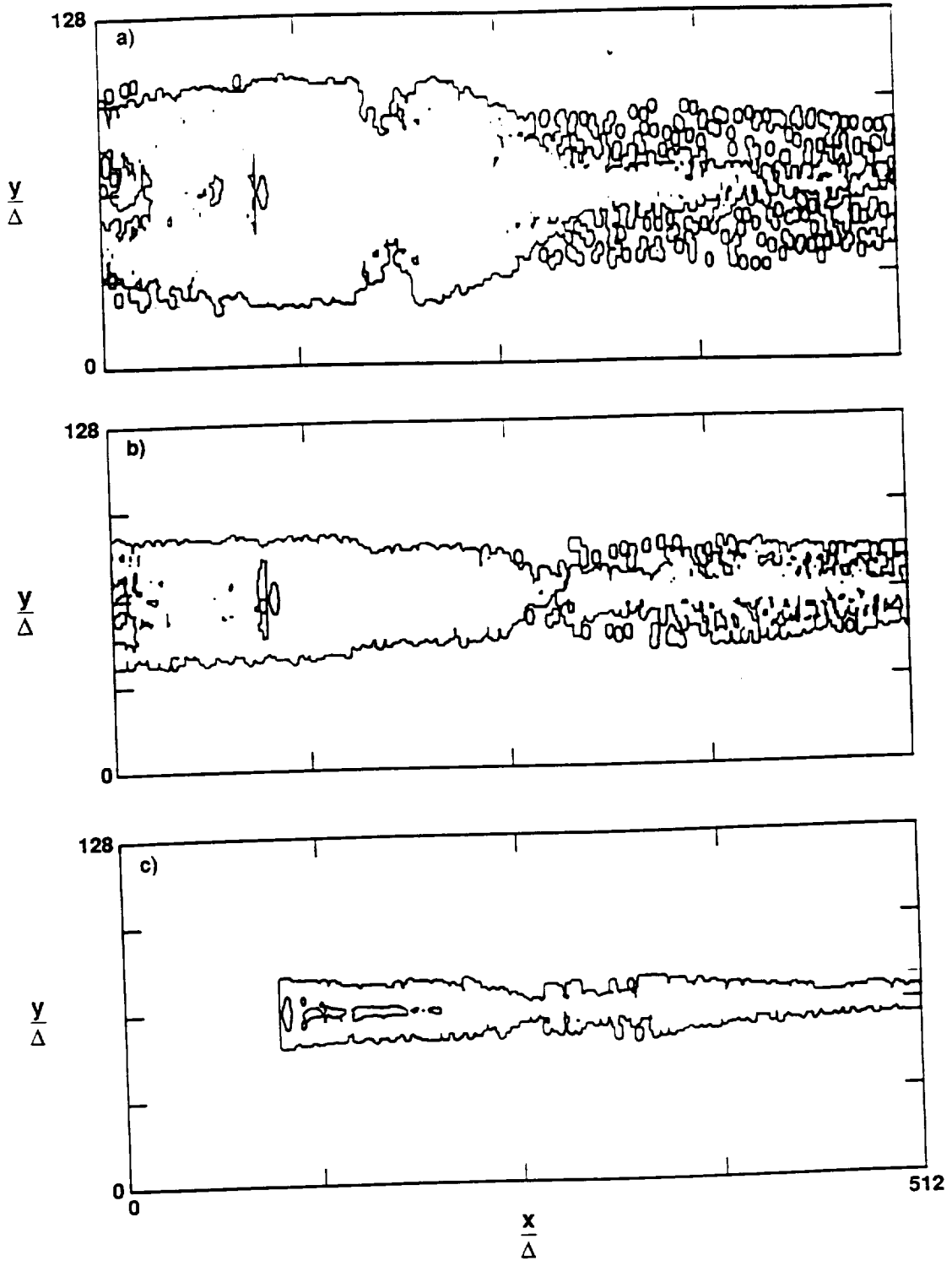


Figure 8

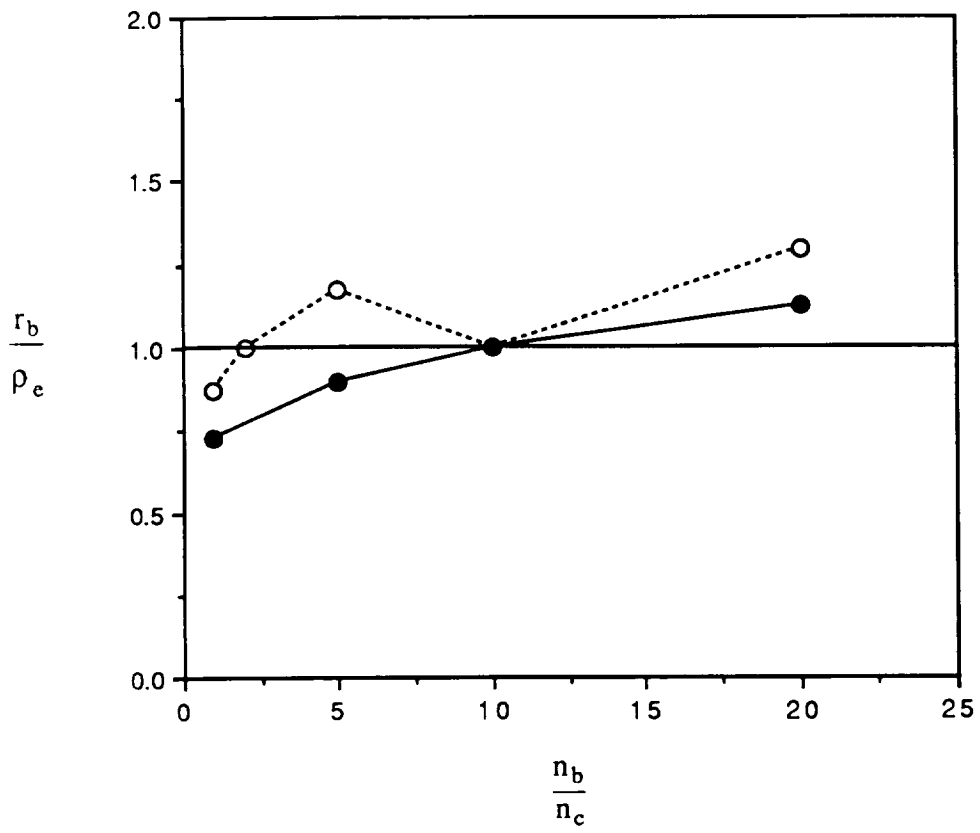


Figure 9

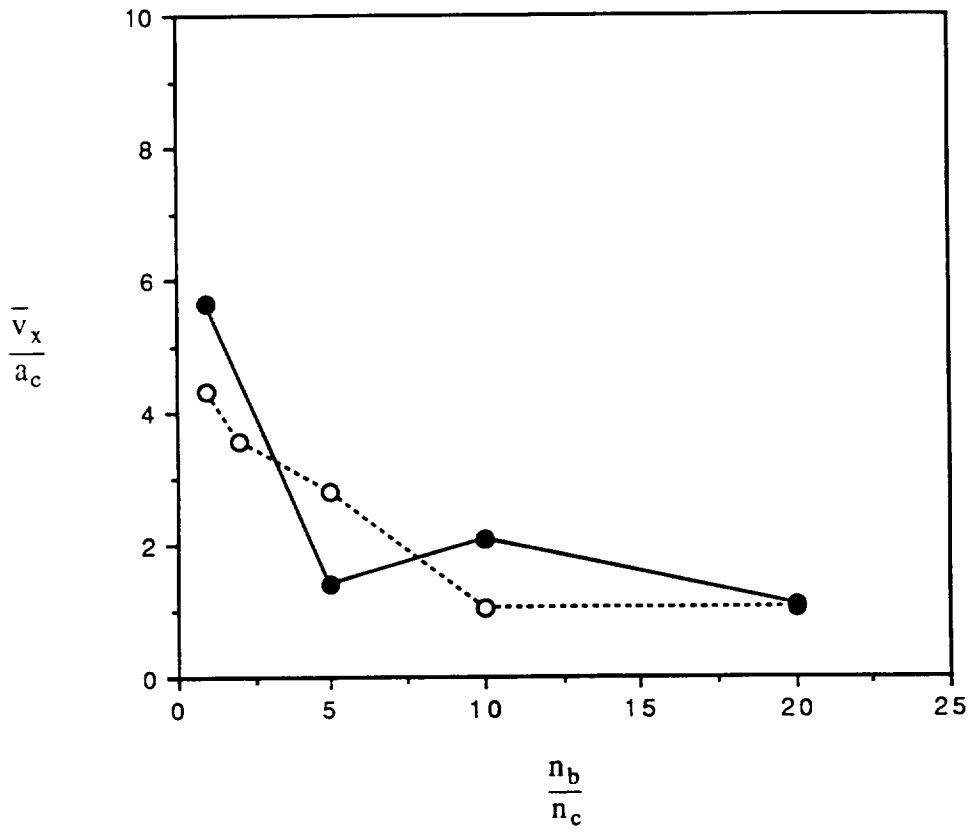


Figure 10

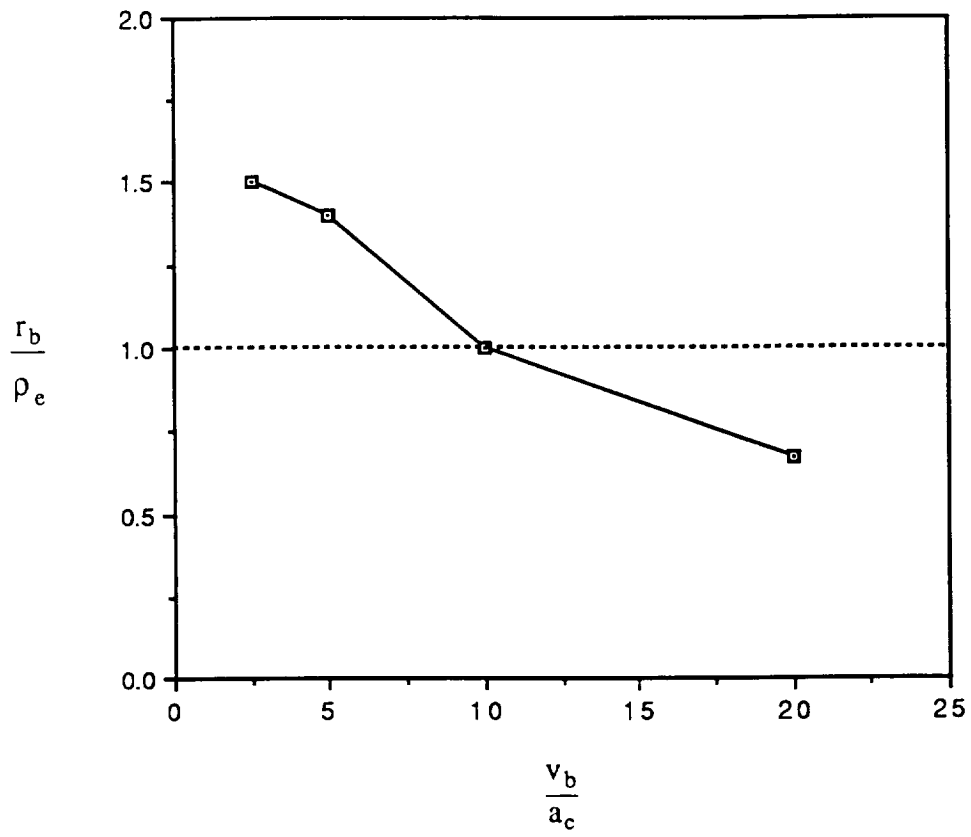


Figure 11

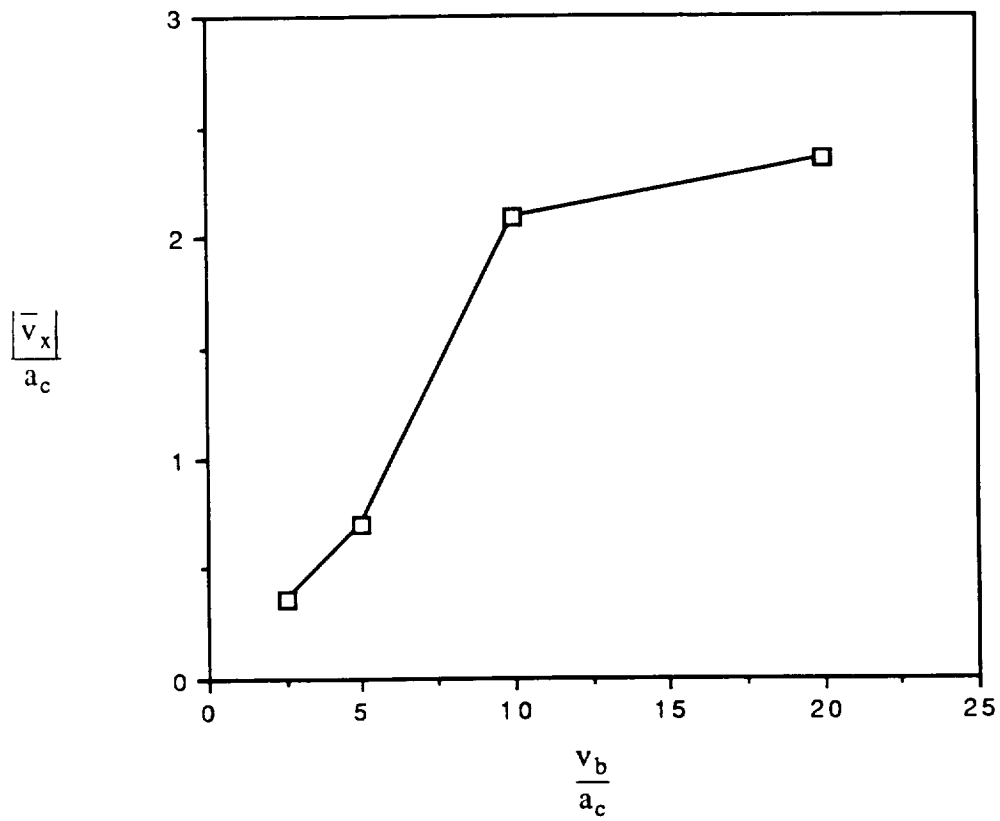


Figure 12

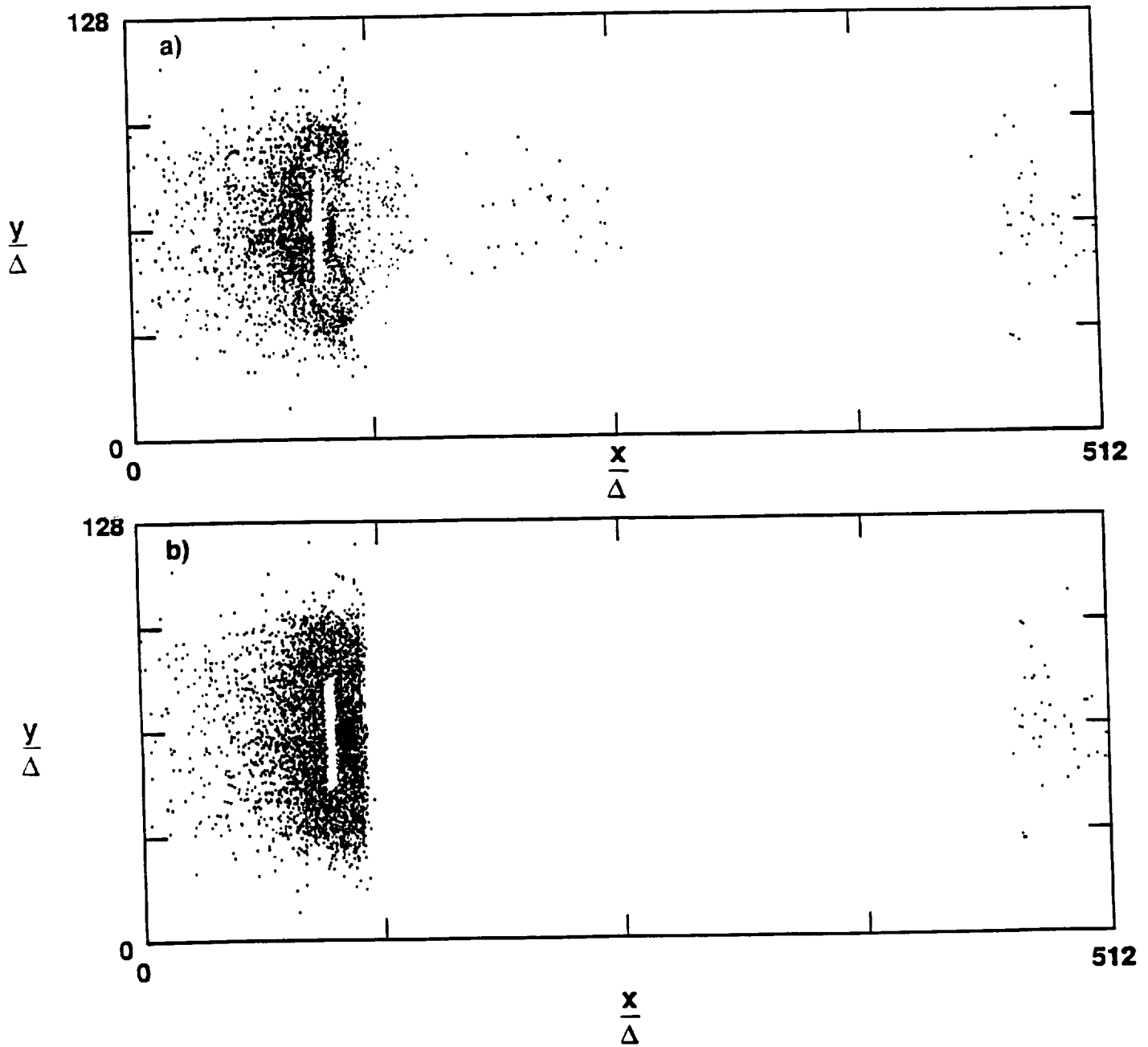


Figure 13

APPENDIX D

**Magnetosheath-ionospheric Plasma Interactions
in the cusp: Meso-particle Simulations**

(Abstract)

MAGNETOSHEATH-IONOSPHERIC PLASMA INTERACTIONS IN THE CUSP:

2. MESO-SCALE PARTICLE SIMULATIONS

R. M. Winglee¹, J. D. Menietti², and C. S. Lin³

¹Geophysics Program AK-50

University of Washington, Seattle 98195

²Department of Physics and Astronomy

University of Iowa, Iowa City, IA 52242

³Department of Space Sciences, P.O. Drawer 28510

Southwest Research Institute, San Antonio, TX 78228

Submitted to J. Geophysical Research

September 30, 1992

ABSTRACT

Ionospheric plasma outflow from the cusp can be an important source of plasma to the magnetosphere. One source of free energy that can drive this outflow is the injection of magnetosheath plasma into the cusp. Two-dimensional (three velocity) meso-scale particle simulations are presented which incorporate global influences such as the convection of plasma across the cusp, the action of the mirror force and the injection of the magnetosheath plasma, combined with wave-particle interactions which produce the actual coupling between the magnetosheath and ionospheric plasmas. It is shown that because the thermal speed of the electrons is higher than the bulk motion of the magnetosheath plasma, an upward current is formed on the equatorward edge of the injection region with return currents on either side. However, the poleward return currents are the stronger due to the convection and mirroring of many of the magnetosheath electrons. The electron distribution in this latter region evolves from upward directed streams to single-sided loss cones or possibly electron conics. The ion distribution also shows a variety of different features depending on its position relative to the injection region due to differences in convection and wave-particle interactions. On the equatorward edge, the distribution has a downflowing magnetosheath component and an upflowing cold ionospheric component due to continuous convection of ionospheric plasma into the region. In the center of the magnetosheath region, heating from the development of an ion-ion streaming instability causes the suppression of the cold ionospheric component and the formation of downward ionospheric streams. Further poleward there is velocity filtering of magnetosheath ions with low pitch angles, so that a ring-beam distribution is formed and which can produce downward ionospheric conics. These downward components can be eventually turned by the mirror force to produce elevated upward conic throughout the region.